arXiv:hep-ex/0703022v1 13 Mar 2007

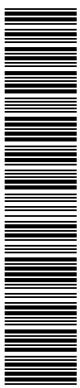# Tests of QCD Factorisation in the Diffractive Production of Dijets in Deep-Inelastic Scattering and Photoproduction at HERA

H1 Collaboration

Abstract

Measurements are presented of differential dijet cross sections in diffractive photoproduction ($Q^2 < 0.01\,\mathrm{GeV}^2$) and deep-inelastic scattering processes (DIS, $4 < Q^2 < 80\,\mathrm{GeV}^2$). The event topology is given by $ep \to eXY$, in which the system X, containing at least two jets, is separated from a leading low-mass proton remnant system Y by a large rapidity gap. The dijet cross sections are compared with NLO QCD predictions based on diffractive parton densities previously obtained from a QCD analysis of inclusive diffractive DIS cross sections by H1. In DIS, the dijet data are well described, supporting the validity of QCD factorisation. The diffractive DIS dijet data are more sensitive to the diffractive gluon density at high fractional parton momentum than the measurements of inclusive diffractive DIS. In photoproduction, the predicted dijet cross section has to be multiplied by a factor of approximately 0.5 for both direct and resolved photon interactions to describe the measurements. The ratio of measured dijet cross section to NLO prediction in photoproduction is a factor 0.5 ± 0.1 smaller than the same ratio in DIS. This suppression is the first clear observation of QCD hard scattering factorisation breaking at HERA. The measurements are also compared to the two soft colour neutralisation models SCI and GAL. The SCI model describes diffractive dijet production in DIS but not in photoproduction. The GAL model fails in both kinematic regions.

A. Aktas[10], V. Andreev[24], T. Anthonis[4], B. Antunovic[25], S. Aplin[10], A. Asmone[32],
A. Astvatsatourov[4], A. Babaev[23,†], S. Backovic[29], A. Baghdasaryan[37], P. Baranov[24],
E. Barrelet[28], W. Bartel[10], S. Baudrand[26], M. Beckingham[10], K. Begzsuren[34], O. Behnke[13],
O. Behrendt[7], A. Belousov[24], N. Berger[39], J.C. Bizot[26], M.-O. Boenig[7], V. Boudry[27],
I. Bozovic-Jelisavcic[2], J. Bracinik[25], G. Brandt[13], M. Brinkmann[10], V. Brisson[26],
D. Bruncko[15], F.W. Büsser[11], A. Bunyatyan[12,37], G. Buschhorn[25], L. Bystritskaya[23],
A.J. Campbell[10], K.B. Cantun Avila[21], F. Cassol-Brunner[20], K. Cerny[31], V. Cerny[15,46],
V. Chekelian[25], A. Cholewa[10], J.G. Contreras[21], J.A. Coughlan[5], G. Cozzika[9], J. Cvach[30],
J.B. Dainton[17], K. Daum[36,42], Y. de Boer[23], B. Delcourt[26], M. Del Degan[39], A. De Roeck[10,44],
E.A. De Wolf[4], C. Diaconu[20], V. Dodonov[12], A. Dubak[29,45], G. Eckerlin[10], V. Efremenko[23],
S. Egli[35], R. Eichler[35], F. Eisele[13], A. Eliseev[24], E. Elsen[10], S. Essenov[23], A. Falkewicz[6],
P.J.W. Faulkner[3], L. Favart[4], A. Fedotov[23], R. Felst[10], J. Feltesse[9,47], J. Ferencei[15], L. Finke[10],
M. Fleischer[10], G. Flucke[11], A. Fomenko[24], G. Franke[10], T. Frisson[27], E. Gabathuler[17],
E. Garutti[10], J. Gayler[10], S. Ghazaryan[37], S. Ginzburgskaya[23], A. Glazov[10], I. Glushkov[38],
L. Goerlich[6], M. Goettlich[10], N. Gogitidze[24], S. Gorbounov[38], M. Gouzevitch[27], C. Grab[39],
T. Greenshaw[17], M. Gregori[18], B.R. Grell[10], G. Grindhammer[25], S. Habib[11,48], D. Haidt[10],
M. Hansson[19], G. Heinzelmann[11], C. Helebrant[10], R.C.W. Henderson[16], H. Henschel[38],
G. Herrera[22], M. Hildebrandt[35], K.H. Hiller[38], D. Hoffmann[20], R. Horisberger[35],
A. Hovhannisyan[37], T. Hreus[4,43], S. Hussain[18], M. Jacquet[26], X. Janssen[4], V. Jemanov[11],
L. Jönsson[19], D.P. Johnson[4], A.W. Jung[14], H. Jung[10], M. Kapichine[8], J. Katzy[10], I.R. Kenyon[3],
C. Kiesling[25], M. Klein[38], C. Kleinwort[10], T. Klimkovich[10], T. Kluge[10], G. Knies[10],
A. Knutsson[19], V. Korbel[10], P. Kostka[38], M. Kraemer[10], K. Krastev[10], J. Kretzschmar[38],
A. Kropivnitskaya[23], K. Krüger[14], M.P.J. Landon[18], W. Lange[38], G. Laštovička-Medin[29],
P. Laycock[17], A. Lebedev[24], G. Leibenguth[39], V. Lendermann[14], S. Levonian[10], L. Lindfeld[40],
K. Lipka[38], A. Liptaj[25], B. List[11], J. List[10], N. Loktionova[24], R. Lopez-Fernandez[22],
V. Lubimov[23], A.-I. Lucaci-Timoce[10], H. Lueders[11], L. Lytkin[12], A. Makankine[8],
E. Malinovski[24], P. Marage[4], Ll. Marti[10], M. Martisikova[10], H.-U. Martyn[1], S.J. Maxfield[17],
A. Mehta[17], K. Meier[14], A.B. Meyer[10], H. Meyer[36], J. Meyer[10], V. Michels[10], S. Mikocki[6],
I. Milcewicz-Mika[6], D. Mladenov[33], A. Mohamed[17], F. Moreau[27], A. Morozov[8], J.V. Morris[5],
M.U. Mozer[13], K. Müller[40], P. Murín[15,43], K. Nankov[33], B. Naroska[11], Th. Naumann[38],
P.R. Newman[3], C. Niebuhr[10], A. Nikiforov[25], G. Nowak[6], K. Nowak[40], M. Nozicka[31],
R. Oganezov[37], B. Olivier[25], J.E. Olsson[10], S. Osman[19], D. Ozerov[23], V. Palichik[8],
I. Panagoulias[l,10,41], M. Pandurovic[2], Th. Papadopoulou[l,10,41], C. Pascaud[26], G.D. Patel[17],
H. Peng[10], E. Perez[9], D. Perez-Astudillo[21], A. Perieanu[10], A. Petrukhin[23], I. Picuric[29],
S. Piec[38], D. Pitzl[10], R. Plačakytė[10], B. Povh[12], P. Prideaux[17], A.J. Rahmat[17], N. Raicevic[29],
P. Reimer[30], A. Rimmer[17], C. Risler[10], E. Rizvi[18], P. Robmann[40], B. Roland[4], R. Roosen[4],
A. Rostovtsev[23], Z. Rurikova[10], S. Rusakov[24], F. Salvaire[10], D.P.C. Sankey[5], M. Sauter[39],
E. Sauvan[20], S. Schätzel[10], S. Schmidt[10], S. Schmitt[10], C. Schmitz[40], L. Schoeffel[9],
A. Schöning[39], H.-C. Schultz-Coulon[14], F. Sefkow[10], R.N. Shaw-West[3], I. Sheviakov[24],
L.N. Shtarkov[24], T. Sloan[16], I. Smiljanic[2], P. Smirnov[24], Y. Soloviev[24], D. South[7],
V. Spaskov[8], A. Specka[27], M. Steder[10], B. Stella[32], J. Stiewe[14], A. Stoilov[33], U. Straumann[40],
D. Sunar[4], T. Sykora[4], V. Tchoulakov[8], G. Thompson[18], P.D. Thompson[3], T. Toll[10],
F. Tomasz[15], D. Traynor[18], T.N. Trinh[20], P. Truöl[40], I. Tsakov[33], G. Tsipolitis[10,41], I. Tsurin[10],
J. Turnau[6], E. Tzamariudaki[25], K. Urban[14], A. Usik[24], D. Utkin[23], A. Valkárová[31], C. Vallée[20],
P. Van Mechelen[4], A. Vargas Trevino[10], Y. Vazdik[24], S. Vinokurova[10], V. Volchinski[37],
K. Wacker[7], G. Weber[11], R. Weber[39], D. Wegener[7], C. Werner[13], M. Wessels[10], Ch. Wissing[10],

1

R. Wolf[13], E. Wünsch[10], S. Xella[40], W. Yan[10], V. Yeganov[37], J. Žáček[31], J. Zálešák[30], Z. Zhang[26], A. Zhelezov[23], A. Zhokin[23], Y.C. Zhu[10], J. Zimmermann[25], T. Zimmermann[39], H. Zohrabyan[37], and F. Zomer[26]

[1] *I. Physikalisches Institut der RWTH, Aachen, Germany[a]*
[2] *Vinca Institute of Nuclear Sciences, Belgrade, Serbia*
[3] *School of Physics and Astronomy, University of Birmingham, Birmingham, UK[b]*
[4] *Inter-University Institute for High Energies ULB-VUB, Brussels; Universiteit Antwerpen, Antwerpen; Belgium[c]*
[5] *Rutherford Appleton Laboratory, Chilton, Didcot, UK[b]*
[6] *Institute for Nuclear Physics, Cracow, Poland[d]*
[7] *Institut für Physik, Universität Dortmund, Dortmund, Germany[a]*
[8] *Joint Institute for Nuclear Research, Dubna, Russia*
[9] *CEA, DSM/DAPNIA, CE-Saclay, Gif-sur-Yvette, France*
[10] *DESY, Hamburg, Germany*
[11] *Institut für Experimentalphysik, Universität Hamburg, Hamburg, Germany[a]*
[12] *Max-Planck-Institut für Kernphysik, Heidelberg, Germany*
[13] *Physikalisches Institut, Universität Heidelberg, Heidelberg, Germany[a]*
[14] *Kirchhoff-Institut für Physik, Universität Heidelberg, Heidelberg, Germany[a]*
[15] *Institute of Experimental Physics, Slovak Academy of Sciences, Košice, Slovak Republic[f]*
[16] *Department of Physics, University of Lancaster, Lancaster, UK[b]*
[17] *Department of Physics, University of Liverpool, Liverpool, UK[b]*
[18] *Queen Mary and Westfield College, London, UK[b]*
[19] *Physics Department, University of Lund, Lund, Sweden[g]*
[20] *CPPM, CNRS/IN2P3 - Univ. Mediterranee, Marseille - France*
[21] *Departamento de Fisica Aplicada, CINVESTAV, Mérida, Yucatán, México[j]*
[22] *Departamento de Fisica, CINVESTAV, México[j]*
[23] *Institute for Theoretical and Experimental Physics, Moscow, Russia[k]*
[24] *Lebedev Physical Institute, Moscow, Russia[e]*
[25] *Max-Planck-Institut für Physik, München, Germany*
[26] *LAL, Université de Paris-Sud 11, IN2P3-CNRS, Orsay, France*
[27] *LLR, Ecole Polytechnique, IN2P3-CNRS, Palaiseau, France*
[28] *LPNHE, Universités Paris VI and VII, IN2P3-CNRS, Paris, France*
[29] *Faculty of Science, University of Montenegro, Podgorica, Montenegro[e]*
[30] *Institute of Physics, Academy of Sciences of the Czech Republic, Praha, Czech Republic[h]*
[31] *Faculty of Mathematics and Physics, Charles University, Praha, Czech Republic[h]*
[32] *Dipartimento di Fisica Università di Roma Tre and INFN Roma 3, Roma, Italy*
[33] *Institute for Nuclear Research and Nuclear Energy, Sofia, Bulgaria[e]*
[34] *Institute of Physics and Technology of the Mongolian Academy of Sciences , Ulaanbaatar, Mongolia*
[35] *Paul Scherrer Institut, Villigen, Switzerland*
[36] *Fachbereich C, Universität Wuppertal, Wuppertal, Germany*
[37] *Yerevan Physics Institute, Yerevan, Armenia*
[38] *DESY, Zeuthen, Germany*
[39] *Institut für Teilchenphysik, ETH, Zürich, Switzerland[i]*
[40] *Physik-Institut der Universität Zürich, Zürich, Switzerland[i]*

1 Introduction

It can be shown in Quantum Chromodynamics (QCD) that the cross section for diffractive processes in deep-inelastic ep scattering (DIS) factorises into universal diffractive parton density functions (DPDFs) of the proton and process-dependent hard scattering cross sections (QCD factorisation) [1]. Diffractive parton densities have been determined from QCD fits to inclusive diffractive cross section measurements in DIS by H1 [2, 3]. It was found that most of the momentum of the diffractive exchange is carried by gluons.

Final state configurations for which a partonic cross section is perturbatively calculable include dijet and heavy quark production, which are directly sensitive to the diffractive gluon distribution. Previous measurements of diffractive dijet production in DIS [4, 5] have been found to be described by leading order (LO) Monte Carlo (MC) QCD calculations based on the factorisation approach that use the diffractive parton densities from [2] and include parton showers to simulate higher order effects. However, using the same diffractive parton densities in LO QCD calculations overestimates the cross section for single-diffractive dijet production in $p\bar{p}$ collisions at the Tevatron by approximately one order of magnitude [6]. This discrepancy has been attributed to the presence of the additional beam hadron remnant in $p\bar{p}$ collisions, which leads to secondary interactions. The suppression, often characterised by a 'rapidity gap survival probability,' cannot be calculated perturbatively but has been parameterised in various ways (see, e.g., [7–11]).

An alternative approach to diffractive scattering is taken by soft colour neutralisation models in which diffraction is described by partonic hard scattering processes with subsequent reconfiguration of colour between the final state partons. One of these models is the Soft Colour Interaction model [12] which, when tuned to describe inclusive diffractive HERA measurements, also gives a reasonable description [13] of diffractive Tevatron data [6, 14–18].

The transition from deep-inelastic scattering to hadron-hadron scattering can be studied at HERA by comparing scattering processes in DIS and in photoproduction. In photoproduction, the beam lepton emits a quasi-real photon which interacts with the proton (γp collision). Processes in which the photon participates directly in the hard scattering are expected to be similar to the deep-inelastic scattering of highly virtual photons ('point-like photon'). In contrast, processes in which the photon is first resolved into partons which then engage in the hard scattering resemble hadron-hadron scattering. These resolved photon processes can produce gluon-gluon and gluon-quark final states, which are present in $p\bar{p}$ collisions but negligible in DIS. Furthermore, they have an additional hadronic remnant which opens up the possibility of remnant-remnant interactions. QCD factorisation is proven for diffractive DIS, is also expected to hold for direct photon interactions in diffractive photoproduction [1], but not for resolved processes. Previous comparisons of diffractive photoproduction dijet data with LO MC models showed consistency with QCD factorisation within large uncertainties [4].

Measurements of diffractive D* meson (charm) production are well described by next-to-leading order (NLO) QCD calculations and by LO Monte Carlo models based on diffractive parton densities in both DIS [19–22] and photoproduction [22]. However, these measurements suffer from large statistical uncertainties of the data.

4

In this paper, a more precise test of QCD factorisation for diffractive dijet production in DIS and photoproduction is presented. Measurements of diffractive dijet cross sections are compared with NLO QCD predictions based on recently published diffractive parton densities [3] from H1. In addition, the dijet cross sections are also compared with two versions of the LO soft colour interaction model. The data were collected with the H1 detector at HERA in the years 1996 and 1997. For photoproduction the integrated luminosity is increased by one order of magnitude with respect to previous results. For DIS, the same data sample is used as in a previous measurement [5]. Jets are defined using the inclusive k_T cluster algorithm [23] with asymmetric cuts on the jet transverse energies to facilitate comparisons with NLO predictions [24, 25]. Apart from the different ranges for the photon virtuality, the DIS and photoproduction measurements are performed in the same kinematic range to allow the closest possible comparison of the results.

2 Kinematics

The generic diffractive positron-proton interaction $ep \to eXY$ is illustrated in Figure 1. The positron (4-momentum k) exchanges a photon (q) which interacts with the proton (P). The produced final state hadrons are, by definition, divided into the systems X and Y, separated by the largest gap in the hadron rapidity distribution relative to the $\gamma^{(*)}p$ collision axis in the photon-proton centre-of-mass frame. The system Y lies in the outgoing proton beam direction.

Examples of direct and resolved photon processes with dijets in the final state are depicted in Figure 2. Resolved processes give a large contribution in photoproduction but are suppressed in DIS. The diffractive exchange in these diagrams is depicted as a pomeron ($\mathbb{P}$).
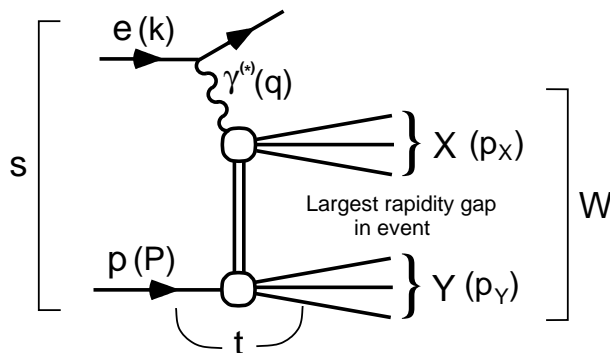
Figure 1: Illustration of the generic diffractive process $ep \to eXY$. The systems X and Y are separated by the largest gap in the rapidity distribution of the final state hadrons.

The usual DIS kinematic variables are defined as:

$$Q^2 \equiv -q^2 , \qquad y \equiv \frac{q \cdot P}{k \cdot P} , \qquad x \equiv \frac{Q^2}{2P \cdot q} . \tag{1}$$
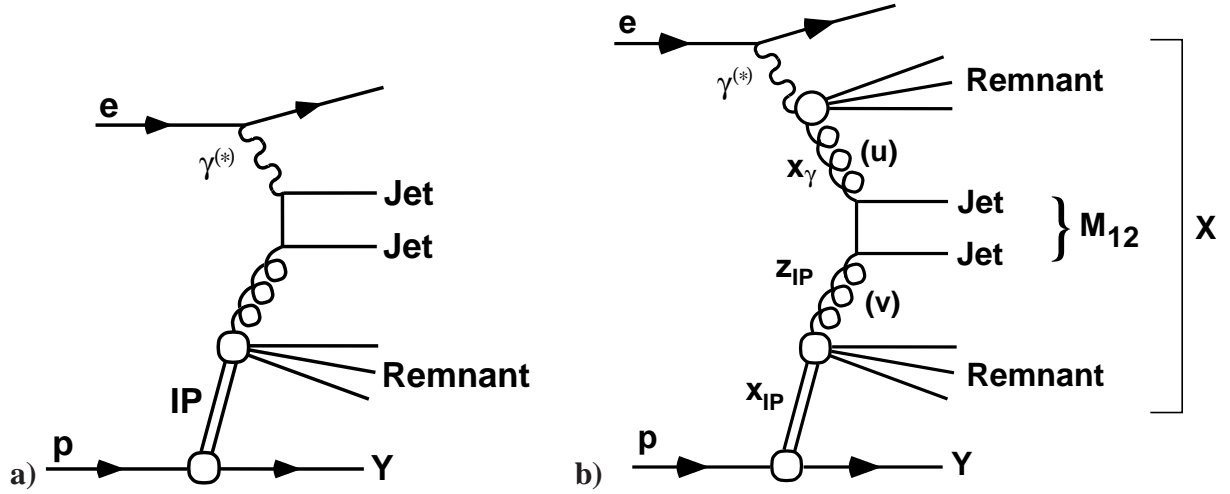
Figure 2: Leading order diagrams for diffractive dijet production at HERA with the diffractive exchange depicted as a pomeron (IP). a) Direct (point-like) photon process (photon-gluon fusion), b) resolved (hadron-like) photon process.

These three variables are related through $Q^2 \approx sxy$, in which $s \equiv (k + P)^2$ is the fixed ep centre-of-mass energy squared. The invariant mass of the photon-proton system W is given by

$$W = \sqrt{(q + P)^2} \approx \sqrt{y\,s - Q^2} \, . \tag{2}$$

With p_X and p_Y representing the 4-momenta of the systems X and Y, we define

$$M_X^2 \equiv p_X^2 \, , \quad M_Y^2 \equiv p_Y^2 \, , \quad t \equiv (P - p_Y)^2 \, , \quad x_{I\!P} \equiv \frac{q \cdot (P - p_Y)}{q \cdot P} \, . \tag{3}$$

The quantities M_X and M_Y are the invariant masses of the systems X and Y, t is the squared four-momentum transferred at the proton vertex and $x_{I\!P}$ represents the fraction of the proton beam momentum transferred to the system X. Diffractive events are characterised by small values of $x_{I\!P}$ ($\lesssim 0.05$). With u and v denoting the four-momenta of the two partons (Figure 2b) or photon and parton (Figure 2a) entering the hard subprocess, the dijet system has squared invariant mass

$$M_{12}^2 = (u + v)^2 \, . \tag{4}$$

The fractional longitudinal momenta carried by the partons from the photon (x_γ) and the diffractive exchange ($z_{I\!P}$) are given by

$$x_\gamma = \frac{P \cdot u}{P \cdot q} \, , \qquad z_{I\!P} = \frac{q \cdot v}{q \cdot (P - p_Y)} \, . \tag{5}$$

The measurements are performed in the region $x_{I\!P} < 0.03$, $-t < 1 \, \mathrm{GeV}^2$ and $M_Y < 1.6 \, \mathrm{GeV}$, where the cross section is dominated by scattering processes in which the proton stays intact.

3 Diffractive Dijet Production in the Factorisation Approach

In the QCD factorisation approach, diffractive ep dijet cross sections are calculated according to the formula

$$\mathrm{d}\sigma(ep \rightarrow e + 2\,\mathrm{jets} + X' + Y) = \sum_{i,j} \int\!\mathrm{d}y\; f_{\gamma/e}(y) \int\!\mathrm{d}x_\gamma\; f_{j/\gamma}(x_\gamma, \mu_F^2)\; \times$$

$$\times \int\!\mathrm{d}t \int\!\mathrm{d}x_{I\!P} \int\!\mathrm{d}z_{I\!P}\; d\hat{\sigma}(ij \rightarrow 2\,\mathrm{jets})\; f_i^D(z_{I\!P}, \mu_F^2, x_{I\!P}, t), \tag{6}$$

in which the sum runs over all contributing partons, $f_{\gamma/e}$ is the photon flux from the positron and $f_{j/\gamma}$ are the photon parton densities. For direct photon interactions, $f_{j/\gamma} = \delta(1 - x_\gamma)$. The partonic cross sections are denoted by $\hat{\sigma}$ and f_i^D are the diffractive parton densities of the proton. The factorisation scale μ_F is assumed to be identical at the photon and proton vertices. In the present analysis, the jet transverse energy is larger than Q for most of the data and is therefore used as the factorisation scale and as the renormalisation scale both in DIS and in photoproduction. The variable X' denotes the part of the hadronic system X which is not contained in the two jets.

The H1 Collaboration has determined diffractive parton densities from QCD fits to inclusive diffractive DIS data in [2, 3]. In the parameterisations used for these fits, the $x_{I\!P}$ and t dependences of the diffractive parton distributions were factorised from the dependences on the scale μ_F and the fractional parton momentum $z_{I\!P}$:

$$f_i^D(z_{I\!P}, \mu_F^2, x_{I\!P}, t) = f_{I\!P}(x_{I\!P}, t)\; f_{i,I\!P}(z_{I\!P}, \mu_F^2). \tag{7}$$

The factor $f_{I\!P}(x_{I\!P}, t)$ was parameterised as suggested by Regge theory. The dependence on $z_{I\!P}$ was parameterised at a starting scale and evolved to the scale at which the inclusive data were measured using the DGLAP evolution equations [26, 27]. The inclusive diffractive DIS data [2,3] are well described using this approach. For $x_{I\!P} > 0.01$, small additional contributions from sub-leading meson ('reggeon') exchange have to be taken into account to describe the data.

The H1 Collaboration has published QCD fits to two different data sets of inclusive diffractive DIS events. In a first analysis [2], data taken in the year 1994 were used to extract the LO 'H1 fit 2' parton densities which have been used previously in comparisons with diffractive dijet production in DIS at HERA and at the Tevatron. A second analysis was based on the larger data samples of the years 1997–2000 [3]. The fit in [3] led to the NLO 'H1 2006 Fit A' and NLO 'H1 2006 Fit B' DPDFs which both give a good description of inclusive diffraction, and which are the basis of the dijet predictions in this paper. The two sets of parton densities differ mainly in the gluon density at high fractional parton momentum, which is poorly constrained by the inclusive diffractive scattering data. The gluon density of Fit A is peaked at the starting scale at high fractional momentum and that of Fit B is flat.

4 Next-to-leading Order QCD Calculations

Existing programs which calculate NLO QCD partonic cross sections for dijet production in inclusive DIS and photoproduction can be adapted to calculate cross sections in diffraction.

For DIS, the DISENT [28] program is used, as suggested in [29]. It was demonstrated in [24, 30, 31] that dijet calculations using this program agree very well with the results from other programs [31–34]. The program by Frixione et al. [35] is used for photoproduction.

The two NLO programs are adapted to calculate diffractive cross sections according to the following procedure. The cross section at fixed $x_{I\!P}$ and $t = 0$ is calculated by reducing the nominal proton beam energy by a factor $x_{I\!P}$. Since the $x_{I\!P}$ and t dependences of the DPDFs are assumed to factorise from the $z_{I\!P}$ and μ_F dependences, the proton PDFs can be replaced by the parton densities of the diffractive exchange $f_{i,I\!P}(z_{I\!P}, \mu_F^2)$. The cross sections are multiplied by $f_{I\!P}(x_{I\!P}, t)$, integrated between $t = -1 \text{ GeV}^2$ and the maximum kinematically allowed value of t. In the same way, a $\approx 3\%$ contribution from Reggeon exchange is calculated. Kinematic effects on the partonic configurations arising from finite values of t are neglected. To compare the results with the measured cross sections in the region $x_{I\!P} < 0.03$, the results are integrated over $x_{I\!P}$.

The diffractive dijet cross sections of the modified programs have been compared at the LO tree level with predictions of the Monte Carlo generator RAPGAP [36] (see also Section 6.4). Good agreement has been found for both DIS and photoproduction, indicating that the diffractive extension works correctly. The diffractive NLO predictions agree with independent calculations in both DIS and photoproduction [37, 38].

For the NLO predictions in this paper, the recent H1 2006 DPDFs are used and the 2-loop strong coupling $\alpha_s(M_Z)$ is set to 0.118; the same value is used in the evolution of the parton densities [3]. The renormalisation scale is set to the transverse energy of the leading parton jet in the photon-proton centre-of-mass frame. In DISENT it is not possible to change the factorisation scale on an event-by-event basis. It is therefore set to the average E_T of the leading jet observed in the DIS measurement (6.2 GeV). Variations of the QCD renormalisation scale by factors 0.5 and 2 in DISENT result in changes of the predicted dijet cross section by approximately $+24\%$ and -17%, respectively, integrated over the DIS kinematic range specified in Table 1. Varying the factorisation scale by factors 0.5 and 2 leads to changes of the predicted dijet cross section by approximately $+8\%$ and -7%, respectively. In the Frixione program for photoproduction, the factorisation and renormalisation scales are fixed to be equal. Variations of the scales by factors 0.5 and 2 change the predicted cross section by approximately $+33\%$ and -21%, respectively, integrated over the photoproduction kinematic range specified in Table 1. In photoproduction, the GRV HO photon PDFs [39] are used. Photon parton densities are not used in DISENT.

The calculated NLO parton jet cross sections are corrected for the effects of hadronisation. The corrections, defined as

$$(1 + \delta_{\text{had}})_i = \left(\frac{\sigma_{\text{dijet}}^{\text{hadron}}}{\sigma_{\text{dijet}}^{\text{parton}}} \right)_i, \tag{8}$$

are determined for both DIS and photoproduction in every measurement bin i using the two Monte Carlo generators RAPGAP with Lund string fragmentation and HERWIG [40] with cluster fragmentation. The HERWIG program was extended to diffraction in the manner described above for the NLO programs and uses LO diffractive parton densities. For the parton level cross section $\sigma_{\text{dijet}}^{\text{parton}}$ the jet algorithm operates on the final state partons after the parton shower cascade. The hadronisation correction is calculated as the mean of the corrections obtained from RAPGAP and HERWIG. The difference between the two corrections serves as an

error estimate. In DIS, the hadron level dijet cross section does not differ significantly from the cross section at the parton level. In photoproduction, the hadron level cross section is lower than the parton level cross section by 10% on average. The correction is particularly large at high x_γ where contributions with $x_\gamma \approx 1$ at the parton level are smeared towards lower values due to hadronisation. The estimated uncertainty on $(1 + \delta_{\mathrm{had}})$ is 20% for $z_{I\!P}^{\mathrm{jets}} > 0.8$ in DIS and less than 10% in all other measurement bins. It is listed in Tables 2–5.

The uncertainty on the parton densities arising from experimental and theoretical uncertainties in the fit to inclusive diffractive data are much smaller than the QCD scale uncertainties of the dijet predictions and are neglected. The NLO corrections increase the LO cross section by factors 1.9 and 1.7 on average in DIS and photoproduction, respectively. This large correction is due to the low transverse energy of the jets.

5 Soft Colour Neutralisation

An approach conceptually different from that of diffractive parton densities is provided by soft colour neutralisation models. In these models, diffractive scattering is described by DIS or photoproduction hard scattering processes with subsequent colour rearrangements between the final state partons. This soft reconfiguration leaves the parton momenta unchanged and can produce colour singlet systems which are separated by a large rapidity gap.

The Soft Colour Interaction model (SCI) [12] contains one free parameter, the colour rearrangement probability, which was fitted to F_2^D measurements. A refined version of the model (GAL) [41] uses a generalised area law for the colour rearrangement probability. Both versions of the model give a reasonably good description [13] of HERA inclusive diffractive cross sections and of diffractive processes at the Tevatron [6, 14–18].

Predictions for diffractive dijet production in the SCI and GAL models are obtained using the LO generator programs LEPTO [42] and PYTHIA [43] for the DIS and photoproduction kinematic regions, respectively. Higher order QCD effects are simulated using parton showers. The calculations are based on the CTEQ5L LO parton densities of the proton [44].

6 Experimental Procedure

6.1 H1 detector

A detailed description of the H1 detector can be found in [45]. Here, a brief account of the components most relevant to the present analysis is given. The H1 coordinate system convention defines the outgoing proton beam direction as the positive z axis, also referred to as the 'forward' direction. The polar angle θ is measured relative to this axis and the pseudorapidity is defined as $\eta \equiv -\ln \tan(\theta/2)$.

The central ep interaction region is surrounded by two large concentric jet drift chambers, two z chambers, and two multi-wire proportional chambers (MWPCs), located inside

a 1.15 T solenoidal magnetic field. Charged particle momenta are measured by the drift chambers in the range $-1.5 < \eta < 1.5$ with a resolution of $\sigma(p_T)/p_T \simeq 0.005\, p_T/\mathrm{GeV} \oplus 0.015$. The MWPCs provide fast trigger information based on the signals of charged particles. In the central and forward region the track detectors are surrounded by a finely segmented Liquid Argon calorimeter (LAr). It consists of an electromagnetic section with lead absorbers and a hadronic section with steel absorbers and covers the range $-1.5 < \eta < 3.4$. The energy resolution is $\sigma(E)/E \simeq 0.11/\sqrt{E/\mathrm{GeV}}$ for electromagnetic showers and $\sigma(E)/E \simeq 0.50/\sqrt{E/\mathrm{GeV}}$ for hadrons, as measured in test beams. The backward region $-4 < \eta < -1.4$ is covered by a lead/scintillating fibre calorimeter (SPACAL) [46] consisting of an electromagnetic and a hadronic section. The electromagnetic part is used to identify and measure the scattered positron in DIS events with an energy resolution of $\sigma(E)/E \simeq 0.07/\sqrt{E/\mathrm{GeV}} \oplus 0.01$. In front of the SPACAL, the Backward Drift Chamber (BDC) provides track segments of charged particles with a resolution of $\sigma(r) = 0.4$ mm and $r\sigma(\phi) = 0.8$ mm.

The forward region is instrumented with the Forward Muon Detector (FMD) and the Proton Remnant Tagger (PRT). Three double layers of drift chambers of the FMD are used to detect particles with pseudorapidities in the range $1.9 < \eta < 3.7$. The FMD can also detect particles from larger pseudorapidities which reach the detector after undergoing secondary scattering with the beam-pipe. The PRT consists of a set of scintillators surrounding the beam pipe at $z = 26$ m and covers the region $6 < \eta < 7.5$.

The ep luminosity is measured with a precision of 1.5% via the Bethe-Heitler Bremsstrahlung process $ep \to ep\gamma$, the photon being detected in a crystal calorimeter at $z = -103$ m. A further crystal calorimeter at $z = -33$ m is used as a small angle positron detector to measure the scattered positron in photoproduction events.

6.2 Event selection

The data correspond to an integrated luminosity of 18 pb^{-1} and were taken in the 1996 and 1997 running periods, in which HERA collided 820 GeV protons with 27.5 GeV positrons. The measurements are described in detail in [47].

The photoproduction data are collected using a trigger which requires the scattered positron to be measured in the small angle positron detector, at least three tracks to be reconstructed in the central jet chambers and an event vertex to be identified. A veto cut requiring less than 0.5 GeV of energy deposited in the photon detector of the luminosity system suppresses initial state radiation and coincidences with Bremsstrahlung events. The geometrical acceptance of the small scattering angle positron detector limits the photon virtuality to $Q^2 < 0.01$ GeV^2 and the photon-proton centre-of-mass energy to $165 < W < 242$ GeV.

DIS events are collected using a trigger which requires the scattered positron to be detected in the backward electromagnetic calorimeter (SPACAL), an event vertex to be identified and at least one high transverse momentum track ($p_T > 0.8$ GeV) to be measured in the central jet chambers. Several cuts are applied on the SPACAL positron candidate to reduce background from photons and hadrons. The electromagnetic cluster energy is required to be larger than 8 GeV and requirements are imposed on the width of the electromagnetic shower, the containment in the electromagnetic section of the SPACAL and an associated track segment in

the BDC. DIS events with initial state QED radiation are suppressed by requiring the summed $E - p_z$ of all final state particles including the positron to be greater than 35 GeV. The range in the photon virtuality is restricted to $4 < Q^2 < 80$ GeV^2. The photon-proton centre-of-mass energy W is restricted to the same range as for photoproduction.

Diffractive events are selected in the same way as for the inclusive diffractive cross section measurement [3] used for the extraction of the DPDFs. No signals above noise thresholds are allowed in the FMD or PRT. In the LAr, no cluster with an energy of more than 400 MeV is allowed in the region $\eta > 3.2$. These selection criteria ensure that the gap between the systems X and Y spans at least the region $3.2 < \eta < 7.5$, and restrict M_Y and t to approximately $M_Y < 1.6$ GeV and $-t < 1$ GeV^2. A cut $x_{I\!P} < 0.03$ further reduces non-diffractive contributions.

The hadronic system X is measured in the LAr and SPACAL calorimeters and the central tracking system. Calorimeter cluster energies and track momenta are combined into hadronic objects using an algorithm which avoids double counting [48]. Jets are formed from the hadronic objects, using the inclusive k_T cluster algorithm [23] with a distance parameter of unity in the photon-proton rest frame, which is identical to the laboratory frame for photoproduction up to a Lorentz boost along the beam axis. The p_T recombination scheme is used, which leads to massless jets. At least two jets are required, with transverse energies $E_T^{*,\mathrm{jet1}} > 5$ GeV and $E_T^{*,\mathrm{jet2}} > 4$ GeV for the leading and sub-leading jet, respectively.[1] The jet axes of the two leading jets are required to lie within the region $-1 < \eta_{\mathrm{jet}}^{\mathrm{lab}} < 2$, well within the acceptance of the LAr calorimeter. The final selection yields 1365 events in photoproduction and 322 events in DIS.

6.3 Kinematic reconstruction

6.3.1 Reconstruction of DIS events

In the DIS analysis, the energy E_e and the polar angle θ_e of the scattered positron are measured in the backward calorimeter SPACAL and y and Q^2 are reconstructed according to

$$y = 1 - \frac{E_e}{E_e^0} \sin^2 \frac{\theta_e}{2}\,, \qquad Q^2 = 4E_e^0 E_e \cos^2 \frac{\theta_e}{2}\,, \tag{9}$$

in which E_e^0 is the positron beam energy. The invariant mass M_X of the hadronic system X is reconstructed from the energies E_i and the momenta $\vec{p}_i$ of all hadronic objects:

$$M_X^2 = \left(\sum_{i \in X} E_i\right)^2 - \left(\sum_{i \in X} \vec{p}_i\right)^2\,. \tag{10}$$

The photon-proton centre-of-mass energy W is reconstructed according to Eq. (2) and the variable $x_{I\!P}$ is given by

$$x_{I\!P} = \frac{Q^2 + M_X^2}{Q^2 + W^2}\,. \tag{11}$$

The estimators x_γ^{jets} and $z_{I\!P}^{\mathrm{jets}}$ of the fractional momenta of the partons entering the hard sub-process are reconstructed as

$$x_\gamma^{\mathrm{jets}} = \frac{\sum_{i=1}^2 \left(E_{\mathrm{jet}\,i}^* - p_{z,\mathrm{jet}\,i}^*\right)}{\sum_{i \in X} \left(E_i^* - p_{z,i}^*\right)}\,, \qquad z_{I\!P}^{\mathrm{jets}} = \frac{Q^2 + M_{12}^2}{Q^2 + M_X^2}\,. \tag{12}$$

---

[1] The '*' denotes variables in the photon-proton rest frame.

6.3.2   Reconstruction of photoproduction events

In the photoproduction analysis, the energy E_e of the scattered positron is measured in the small scattering angle positron detector and y is reconstructed according to

$$y = 1 - E_e/E_e^0. \tag{13}$$

The estimators x_γ^{jets} and $z_{I\!P}^{\text{jets}}$ are reconstructed as

$$x_\gamma^{\text{jets}} = \frac{\sum_{i=1}^2 \left(E_{\text{jet }i} - p_{z,\text{jet }i}\right)}{2\,y\,E_e^0}, \qquad z_{I\!P}^{\text{jets}} = \frac{\sum_{i=1}^2 \left(E_{\text{jet }i} + p_{z,\text{jet }i}\right)}{2\,x_{I\!P}\,E_p}, \tag{14}$$

in which E_p is the incident proton beam energy. The variable $x_{I\!P}$ is reconstructed according to

$$x_{I\!P} = \frac{\sum_{i \in X}\left(E_i + p_{z,i}\right)}{2\,E_p}. \tag{15}$$

The reconstruction of $z_{I\!P}^{\text{jets}}$ and $x_{I\!P}$ is different from the DIS case due to the large contribution of resolved photon processes.

6.4   Monte Carlo simulations

Monte Carlo programs are used in the analysis to correct the measured distributions for detector effects. The H1 detector response is simulated using detailed detector simulation programs based on GEANT [49]. The Monte Carlo events are subjected to the same analysis chain as the data.

The main Monte Carlo generator used to correct the data distributions is RAPGAP [36]. Events are generated according to a convolution of LO diffractive parton densities with LO QCD matrix elements for the hard $2 \to 2$ subprocess. The 'H1 fit 2' DPDFs of [2] are used. RAPGAP includes resolved photon processes for which the partonic cross sections are also convoluted with the parton densities of the photon. In photoproduction, the leading order GRV '94 parton distribution functions [39] are used, which were found to give a good description of the effective photon structure function as measured by H1 [50]. For DIS, processes with a resolved virtual photon are generated using the SAS-2D parameterisation [51], which leads to a reasonable description of inclusive dijet production [52] in a similar Q^2 and E_T range to that studied here. The PDFs are taken at the scale $\mu_F^2 = \hat{p}_T^2 + 4m_q^2$, where $\hat{p}_T$ is the transverse momentum of the emerging hard partons and m_q is the mass of the quarks produced. Higher order effects are simulated using parton showers [53] in the leading $\log(\mu)$ approximation. The Lund string model [54] is used for hadronisation. Photon radiation from the positron lines is simulated using the program HERACLES [55]. The used RAPGAP version simulates only processes in which the proton stays intact.

6.5 Cross section measurement

The data are first corrected for losses at the trigger level. The trigger efficiency is approximately 90% in DIS, the losses being mainly due to the tracking requirements. In photoproduction the efficiency also depends on the energy of the positron detected in the small scattering angle detector and varies between $\approx 90\%$ at low y and $\approx 50\%$ at high y. Non-diffractive background migrating into the measurement region from $M_Y > 5$ GeV and large $x_{I\!P}$ is statistically subtracted using inclusive dijet production simulations (RAPGAP in DIS and PYTHIA in photoproduction). The subtracted background amounts to 3% in photoproduction and 5% in DIS. Due to the limited geometrical detector acceptance in the forward direction it is not possible to distinguish an intact final state proton from one which dissociates into a low-mass system Y. Thus the measured cross section is defined to include proton dissociation with $M_Y < 1.6$ GeV. The correction factor for migrations about the measurement boundary $M_Y = 1.6$ GeV is determined using the DIFFVM [56] simulation of proton dissociation in the range $m_p < M_Y < 5$ GeV. In the simulation, the ratio of elastic proton to proton dissociation cross sections is assumed to be unity, in accordance with the inclusive measurements of [3, 57]. The correction factors are found to be 0.96 ± 0.04 for the 1996 running period and 0.92 ± 0.05 in 1997, the difference resulting from the degrading performance of the detectors used to veto proton dissociation. An additional factor 1.055 ± 0.014 is applied to account for the loss of diffractive events due to noise fluctuations in the FMD. This factor is determined using randomly triggered events. A correction of 5% is applied to compensate for the removal of dijet events in which a bremsstrahlung process is overlaid. A small correction ($< 1\%$) is applied to the measured DIS cross section to account for QED radiation effects.

The final jet cross sections are given at the hadron level. The measured distributions at the detector level are corrected for detector inefficiencies, acceptances and migrations between measurement intervals in the reconstruction using the RAPGAP Monte Carlo program and applying a bin-to-bin correction. The simulation gives a good description of the shapes of all data distributions and of the energy flow in the events. Figure 3 shows the transverse energy flow around the axis of the leading jet for the selected diffractive dijets in DIS (Figure 3a,b) and photoproduction (Figure 3c,d). A clear back-to-back structure is visible in the $\Delta\Phi^*$ distribution. The transverse energy flow in the jets as well as in the region between the jets is reasonably well described by the simulation.

According to the simulations, the detector level observables are well correlated with the hadron level quantities. Purities and stabilities[2] are larger than 25%, the main source of migrations being the jet transverse energy measurements.

The cross sections are measured in the kinematic region specified in Table 1. The pseudo-rapidity range $-3 < \eta^* < 0$ in the photon-proton rest frame used for the DIS measurement corresponds approximately to the range $-1 < \eta < 2$ in the laboratory frame.

---

[2]'Purity' is defined as the fraction of Monte Carlo simulated events reconstructed in a certain measurement interval that are also generated in that bin. 'Stability' is defined as the fraction of events generated in a bin that are also reconstructed in that bin.
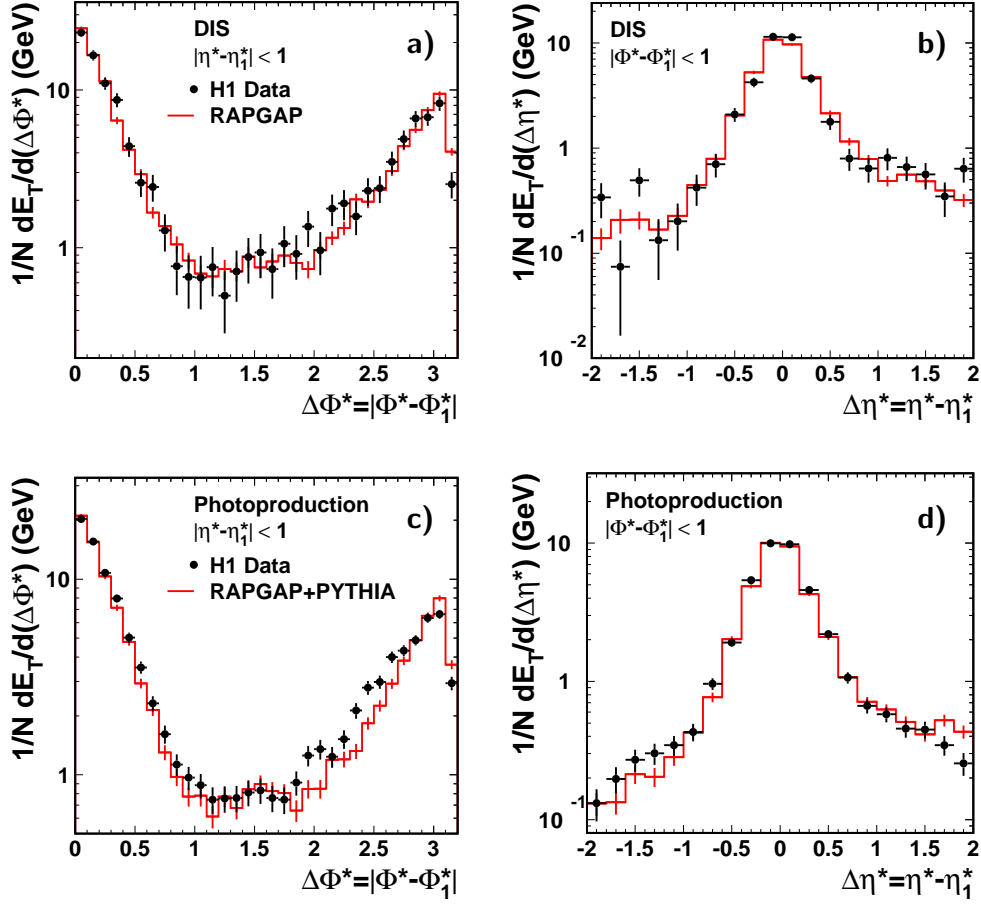
Figure 3: Average transverse energy flow per event around the leading jet axis for diffractive dijets at the detector level in DIS (a and b) and photoproduction (c and d). The variables $\Delta\eta^*$ and $\Delta\Phi^*$ denote the distances from the axis of the leading jet in pseudorapidity and azimuth in the photon-proton rest frame, respectively. In a) and c) only energy within one unit of pseudorapidity around the jet axis is included whereas the profiles b) and d) include energy within one unit in azimuth around the axis.

6.6 Analysis of systematic uncertainties

The following systematic errors on the measured cross sections arise from experimental sources such as detector calibration uncertainties. The cross section errors are estimated by repeating the analysis with variations in the reconstruction of detector-simulated Monte Carlo events.

- A 4% uncertainty in the absolute energy scale of the hadronic LAr calorimeter in the jet E_T range considered here [58] affects the reconstruction of the hadronic final state. The resulting uncertainty on the measured cross section is 4% in DIS and 8% in photoproduction and is strongly correlated between the data points. The influence of this uncertainty in DIS and in photoproduction is different due to the different reconstruction of $x_{I\!\!P}$. A 7% uncertainty in the SPACAL hadronic energy scale affects the cross sections by 1%. The uncertainty in the fraction of the energy of the reconstructed hadronic objects which is carried by tracks is 3% and gives rise to errors on the cross section of 4% in photoproduction and 3% in DIS, again strongly correlated between data points.

14

Photoproduction	DIS
$Q^2 < 0.01$ GeV^2	$4 < Q^2 < 80$ GeV^2
$165 < W < 242$ GeV	
inclusive k_T jet algorithm, distance parameter $= 1$	
$N_{\mathrm{jet}} \geq 2$	
$E_T^{*,\mathrm{jet}\,1} > 5$ GeV	
$E_T^{*,\mathrm{jet}\,2} > 4$ GeV	
$-1 < \eta_{\mathrm{jet}(1,2)} < 2$	$-3 < \eta^*_{\mathrm{jet}(1,2)} < 0$
$x_{I\!P} < 0.03$	
$M_Y < 1.6$ GeV	
$-t < 1$ GeV^2	

Table 1: The kinematic ranges of the measured hadron level ep cross sections.

- The absolute SPACAL electromagnetic energy scale is known to 0.3% for scattered positrons with $E_e = 27.5$ GeV and 2.0% at $E_e = 8$ GeV. The polar scattering angle of the positron is measured to 1 mrad precision. The uncertainties of the positron energy and angle measurements in DIS result in cross section errors in the range of 4 to 5% for the energy uncertainty and 2% for the scattering angle. In photoproduction, the uncertainty in the knowledge of the acceptance and efficiency of the small angle positron detector results in a cross section error of 5% on average.

- The uncertainties on the trigger efficiencies and the luminosity measurement give rise to cross section uncertainties of 6% and 1.5%, respectively.

- An uncertainty of 25% in the fraction of events lost due to noise in the FMD translates into a 1.3% normalisation error on the cross section.

Systematic errors arising from uncertainties in the acceptance and migration corrections are estimated by repeating the measurements with variations in the kinematic dependences and other details of the Monte Carlo models within experimentally allowed limits.

- The shapes of the following distributions in the RAPGAP simulation have been varied: a) the $z_{I\!P}$ distribution in photoproduction has been reweighted by factors $z_{I\!P}^{\pm 0.3}$ and $(1 - z_{I\!P})^{\pm 0.3}$; b) the $E_T^{\mathrm{jet}\,1}$ distribution by $\hat{p}_T^{\pm 0.5}$ in both photoproduction and DIS; c) the $x_{I\!P}$ distribution by $x_{I\!P}^{\pm 0.2}$ in photoproduction and $x_{I\!P}^{\pm 0.3}$ in DIS; d) the x_γ distribution by $x_\gamma^{\pm 0.3}$ and $(1 - x_\gamma)^{\pm 0.3}$ in both kinematic regions and e) the y distribution by $y^{\pm 0.5}$ and $(1 - y)^{\pm 0.5}$ in both kinematic regions. In DIS, the largest deviation (9%) is due to the $x_{I\!P}$ reweighting. In photoproduction the largest error (6%) arises from the $\hat{p}_T$ reweighting.

- The t distribution is varied by factors $e^{\pm 2t/\mathrm{GeV}^2}$ as constrained by inclusive measurements [57,59] leading to cross section errors of 2 to 3%.

- The estimated number of non-diffractive background events which migrate into the sample from the unmeasured region $x_{I\!P} > 0.03$ or $M_Y > 5$ GeV is varied by $\pm 50\%$, leading to a mean cross section uncertainty of 2% in photoproduction and 3% in DIS.

- A 7% error arises from uncertainties in the migrations about the M_Y boundary of the measurement. It is estimated by varying the simulated efficiencies of the forward detectors FMD and PRT by $\pm 4\%$ and $\pm 25\%$, respectively, and by variations in the DIFFVM simulation of a) the ratio of elastic proton to proton dissociation cross sections between $1:2$ and $2:1$, b) the generated M_Y distribution within $M_Y^{-2.0\pm0.3}$, c) the t dependence in the proton dissociation simulation by factors $e^{\pm t/\mathrm{GeV}^2}$.

- The loss of diffractive events due to the η_{max} cut and the cuts on the FMD and PRT is corrected using the RAPGAP simulation. By studying jet events with an elastically scattered proton (measured in a Roman pot detector) in the range $x_{I\!P} < 0.05$, it is established that the RAPGAP simulation describes the loss seen in the data within a 10% and 14% statistical uncertainty for photoproduction and DIS, respectively [60]. This uncertainty is used to estimate the uncertainty on the rapidity gap selection in the present analysis and translates into cross section errors of 1% in both photoproduction and DIS.

The largest errors in photoproduction arise from the uncertainty in the LAr energy scale and the migrations about the M_Y boundary. In DIS, the largest error arises from the $x_{I\!P}$ reweighting of RAPGAP. The uncertainties due to the LAr hadronic energy scale, the energy contribution of tracks, the luminosity, the FMD noise, the estimated number of background events and the positron energy in the SPACAL for DIS are correlated between cross section bins. Both for the bin-to-bin correlated and the uncorrelated errors all individual contributions are added in quadrature to obtain the full uncertainties.

7   Results

The measurement results are presented in Figures 4–12 and are listed in Tables 2–5 as bin-averaged differential hadron level cross sections for a set of kinematic variables which characterise the scattering process. The measurements are compared with next-to-leading order QCD predictions based on the factorisation approach in Sections 7.1–7.4 and to leading order soft colour neutralisation models in Section 7.5.

7.1   Diffractive dijet production in DIS

In Figures 4 and 5, the differential cross sections are shown as functions of $z_{I\!P}^{\mathrm{jets}}$, $\log_{10}(x_{I\!P})$, W, Q^2, $E_T^{*,\mathrm{jet1}}$, $\langle \eta_{\mathrm{jet}}^{\mathrm{lab}} \rangle$, and $\left| \Delta \eta_{\mathrm{jet}}^* \right|$. The data are compared with NLO QCD predictions obtained using the DISENT program with the 'H1 2006 Fit A' and 'H1 2006 Fit B' diffractive parton densities.

The NLO prediction based on the 'H1 2006 Fit A' parton densities (only shown in Figure 4) overestimates the measured cross section, in particular at high $z_{I\!P}^{\mathrm{jets}}$. The NLO prediction based on the 'H1 2006 Fit B' parton densities agrees well with the distributions of all variables within the given errors. Hence the dijet cross sections distinguish between the two parton density sets which describe inclusive diffractive DIS similarly well. The good description of the differential cross section as a function of $\log_{10}(x_{I\!P})$ indicates that the $x_{I\!P}$ dependence of $f_{I\!P}(x_{I\!P}, t)$ is compatible with the dijet production mechanism within the shown errors. The agreement between predicted and measured differential cross sections as functions of $E_T^{*,\mathrm{jet1}}$ and $\left|\Delta\eta_{\mathrm{jet}}^*\right|$ suggests that the NLO QCD matrix element describes the hard scatter correctly within the uncertainties shown. The good description of both inclusive diffractive scattering and diffractive dijet production obtained from the 'H1 2006 Fit B' parton densities supports the validity of QCD hard scattering factorisation in diffractive DIS. In the following discussion of diffractive dijet photoproduction, only the 'H1 2006 Fit B' densities are considered.

7.2   Diffractive photoproduction of dijets

Differential cross sections measured for photoproduction are shown in Figure 6 as functions of $z_{I\!P}^{\mathrm{jets}}$ and $x_{\gamma}^{\mathrm{jets}}$. The measurements are compared with NLO predictions obtained with the Frixione et al. program, interfaced to the 'H1 2006 Fit B' diffractive parton densities.

The NLO prediction overestimates the measured dijet cross section by a factor of approximately 2. Diffractive dijet photoproduction thus cannot be described using the parton densities which lead to a good description of diffractive scattering in DIS. QCD hard scattering factorisation is therefore broken in photoproduction. A more detailed comparison of the cross sections in DIS and photoproduction is given in the next section.

7.3   Ratio of dijet cross sections in diffractive photoproduction and DIS

A reliable method to test QCD factorisation is obtained by dividing the ratio of measured to predicted cross sections in photoproduction by the corresponding ratio in DIS. In this double ratio many experimental errors and also theoretical scale errors cancel to a large extent. The double ratio is shown in Figure 7 as a function of the photon-proton centre-of-mass energy W. The two NLO calculations are based on the 'H1 2006 Fit B' diffractive parton densities and are corrected for hadronisation. The double ratio is rather insensitive to the detailed shape of the diffractive gluon density and the conclusions remain unchanged if the 'H1 2006 Fit A' parton densities are used.

The double ratio is ≈ 0.5 throughout the measured W range, indicating a suppression factor which is independent of the centre-of-mass energy within the uncertainties. Integrated over the measured kinematic range the ratio of data to NLO expectation for photoproduction is a factor 0.5 ± 0.1 smaller than the same ratio in DIS where the error includes scale uncertainties. This confirms that QCD hard scattering factorisation is broken for diffractive dijet production in photoproduction with respect to the same process in DIS. The suppression in photoproduction is much smaller than the suppression in diffractive dijet production at the Tevatron [6].

7.4 Study of QCD factorisation breaking in photoproduction

The simple assumption that the suppression factor in photoproduction does not depend on any kinematic variable is studied by scaling the NLO predictions by an overall suppression factor 0.5. Using such a global factor for both resolved and direct photon processes leads to a good description of all measured distributions as shown in Figures 8 and 9.

Whilst a suppression of resolved photoproduction is generally expected, a suppression of the direct photon contribution is in contradiction to theoretical expectations [1]. At NLO, the contributions of direct and resolved photon processes to the dijet cross section cannot be calculated separately. The following discussion therefore focuses on the dependence of the suppression on the variable $x_{\gamma,\mathrm{PL}}^{\mathrm{jets}}$, reconstructed at the parton level (PL) from parton jets before hadronisation, which is related to the fraction of the photon energy entering the jet system. In events with $x_{\gamma,\mathrm{PL}}^{\mathrm{jets}} > 0.9$ almost the entire photon energy enters the jet system, whereas for events with $x_{\gamma,\mathrm{PL}}^{\mathrm{jets}} < 0.9$ a significant photon remnant system is present which may lead to secondary interactions and rapidity gap destruction. A fit of the NLO prediction to the cross section differential in x_γ^{jets} with two free normalisation parameters for contributions from $x_{\gamma,\mathrm{PL}}^{\mathrm{jets}} < 0.9$ and $x_{\gamma,\mathrm{PL}}^{\mathrm{jets}} > 0.9$ yields suppression factors of 0.47 ± 0.16 and 0.53 ± 0.14, respectively. This result indicates again that the suppression is independent of $x_{\gamma,\mathrm{PL}}^{\mathrm{jets}}$ and that both direct and resolved contributions have to be suppressed by the same factor.

Finally an investigation is performed of how well the data can be described under the assumption that the NLO calculation with $x_{\gamma,\mathrm{PL}}^{\mathrm{jets}} > 0.9$ is not suppressed. The best agreement in a χ^2 fit is reached for a suppression factor 0.44 for the NLO calculation with $x_{\gamma,\mathrm{PL}}^{\mathrm{jets}} < 0.9$ and the resulting distributions are shown for x_γ^{jets}, W, $\langle \eta_{\mathrm{jet}} \rangle$ and $E_T^{\mathrm{jet}\,1}$ in Figure 10. This prediction is incompatible with the measured cross sections. The assumption that the direct part obeys QCD factorisation is therefore strongly disfavoured by the present analysis.

7.5 Leading order soft colour neutralisation models

The predictions of the soft colour interaction models SCI and GAL using the CTEQ5L LO parton densities of the proton are compared with the measurements in Figure 11 in the DIS kinematic region. The SCI model describes the dijet cross section reasonably well. If the GRV '94 HO proton parton densities [61] are used the cross sections are underestimated by a factor of approximately 2 in agreement with the conclusions drawn in [5]. The GAL model overestimates the dijet rate by about 65% on average. It gives a good description of the shapes of the differential cross sections as functions of W and $\langle \eta_{\mathrm{jet}}^{\mathrm{lab}} \rangle$ but not as functions of $z_{I\!\!P}^{\mathrm{jets}}$ and $\log_{10}(x_{I\!\!P})$.

The predictions for photoproduction are shown in Figure 12. The normalisation of the cross section is underestimated by factors of approximately 2.2 for the SCI model and 1.5 in the case of the GAL model. Both models describe the shapes of the differential cross sections reasonably well for $\log_{10}(x_{I\!\!P})$, W and x_γ^{jets} but fail for $z_{I\!\!P}^{\mathrm{jets}}$.

In summary, neither of the two models which describe diffractive dijet production in $p\bar{p}$ collisions is able to describe it in both DIS and photoproduction.

8 Summary

Diffractive dijet production is measured in deep-inelastic scattering and photoproduction in the same kinematic range $165 < W < 242$ GeV, $x_{I\!P} < 0.03$, $E_T^{*,\text{jet}1} > 5$ GeV and $E_T^{*,\text{jet}2} > 4$ GeV, with limits on the photon virtuality $4 < Q^2 < 80$ GeV^2 for DIS and $Q^2 < 0.01$ GeV^2 for photoproduction. The inclusive k_T cluster algorithm is used in the definition of the jets.

In DIS, diffractive dijet production is well described within the experimental and theoretical uncertainties by NLO calculations based on diffractive parton densities determined from QCD fits to inclusive diffractive DIS data. QCD factorisation therefore holds within present uncertainties in diffractive DIS. The dijet measurements clearly favour the 'H1 2006 Fit B' over the 'H1 2006 Fit A' parton densities, both of which lead to a good description of inclusive diffraction. The gluon densities from the two sets differ mainly for high fractional momentum. In this region, the dijet cross section is more sensitive to the diffractive gluon density than the inclusive scattering cross section.

In photoproduction, NLO calculations based on the 'H1 2006 Fit B' parton densities overestimate the measured cross section. The ratio of measured cross section to NLO prediction is a factor 0.5 ± 0.1 smaller than the same ratio in DIS, indicating a clear break-down of QCD factorisation. A fit to the photoproduction data yields suppression factors of 0.47 ± 0.16 for the part of the NLO calculation for which $x_{\gamma,\text{PL}}^{\text{jets}} < 0.9$ and 0.53 ± 0.14 for $x_{\gamma,\text{PL}}^{\text{jets}} > 0.9$, where $x_{\gamma,\text{PL}}^{\text{jets}}$ is the fraction of the photon momentum entering the hard scatter and is reconstructed at the parton level from parton jets before hadronisation. The two factors are compatible with each other, indicating that the suppression is independent of $x_{\gamma,\text{PL}}^{\text{jets}}$. Direct photon processes contribute primarily at highest values of $x_{\gamma,\text{PL}}^{\text{jets}}$ and the present analysis therefore indicates that they are suppressed by a similar factor as resolved photon processes. A suppression of direct photon processes cannot be explained by models which base the rapidity gap survival probability on the presence of photon spectator interactions.

The dijet cross sections are also compared with predictions of two soft colour neutralisation models. The SCI model which describes diffractive structure functions at HERA and diffractive dijet production at the Tevatron reproduces DIS dijet cross sections reasonably well but fails for photoproduction both in normalisation and in the shape of the differential cross section in $z_{I\!P}^{\text{jets}}$. The GAL model is incompatible with both data sets.

Acknowledgements

References

[1] J. Collins, *Phys. Rev.* **D57** (1998) 3051 and erratum ibid. **D61** (2000) 019902 [hep-ph/9709499].

[2] H1 Collaboration, C. Adloff *et al.*, *Z. Phys.* **C76** (1997) 613 [hep-ex/9708016].

[3] H1 Collaboration, A. Aktas *et al.*, *Eur. Phys. J.* **C48** (2006) 715 [hep-ex/0606004].

[4] H1 Collaboration, C. Adloff *et al.*, *Eur. Phys. J.* **C6** (1999) 421 [hep-ex/9808013].

[5] H1 Collaboration, C. Adloff *et al.*, *Eur. Phys. J.* **C20** (2001) 29 [hep-ex/0012051].

[6] CDF Collaboration, T. Affolder *et al.*, *Phys. Rev. Lett.* **84** (2000) 5043.

[7] J. D. Bjorken, *Phys. Rev.* **D47** (1993) 101.

[8] E. Gotsman, E. Levin, U. Maor, *Phys. Lett.* **B309** (1993) 199 [hep-ph/9302248].

[9] E. Gotsman, E. Levin, U. Maor, *Phys. Lett.* **B438** (1998) 229 [hep-ph/9804404].

[10] B. Cox, J. Forshaw, L. Lönnblad, *J. High Energy Phys.* **JHEP 10** (1999) 23 [hep-ph/9908464].

[11] A. Kaidalov *et al.*, *Phys. Lett.* **B567** (2003) 61 [hep-ph/0306134].

[12] A. Edin, G. Ingelman, J. Rathsman, *Phys. Lett.* **B366** (1996) 371 [hep-ph/9508386];
A. Edin, G. Ingelman, J. Rathsman, *Z. Phys.* **C75** (1997) 57 [hep-ph/9605281].

[13] R. Enberg, G. Ingelman, N. Timneanu, *Phys. Rev.* **D64** (2001) 114015 [hep-ph/0106246].

[14] CDF Collaboration, F. Abe *et al.*, *Phys. Rev. Lett.* **78** (1997) 2698 [hep-ex/9703010].

[15] CDF Collaboration, T. Affolder *et al.*, *Phys. Rev. Lett.* **84** (2000) 232.

[16] CDF Collaboration, F. Abe *et al.*, *Phys. Rev. Lett.* **79** (1997) 2636.

[17] D0 Collaboration, B. Abbott *et al.*, *Phys. Lett.* **B531** (2002) 52 [hep-ex/9912061].

[18] CDF Collaboration, T. Affolder *et al.*, *Phys. Rev. Lett.* **85** (2000) 4215.

[19] H1 Collaboration, C. Adloff *et al.*, *Phys. Lett.* **B520** (2001) 191 [hep-ex/0108047].

[20] ZEUS Collaboration, S. Chekanov *et al.*, *Phys. Lett.* **B545** (2002) 244 [hep-ex/0206020].

[21] ZEUS Collaboration, S. Chekanov *et al.*, *Nucl. Phys.* **B672** (2003) 3 [hep-ex/0307068].

[22] H1 Collaboration, A. Aktas *et al.*, DESY-06-164, accepted by *Eur. Phys. J.* **C** [hep-ex/0610076].

[23] S. Ellis, D. Soper, *Phys. Rev.* **D48** (1993) 3160 [hep-ph/9305266];
S. Catani *et al.*, *Nucl. Phys.* **B406** (1993) 187.

[24] B. Pötter, *Comp. Phys. Commun.* **133** (2000) 105 [hep-ph/9911221].

[25] M. Klasen, G. Kramer, *Phys. Lett.* **B366** (1996) 385 [hep-ph/9508337];
S. Frixione, G. Ridolfi, *Nucl. Phys.* **B507** (1997) 315 [hep-ph/9707345].

[26] V. Gribov, L. Lipatov, *Sov. J. Nucl. Phys.* **15** (1972) 438, 675;
Y. Dokshitzer, *Sov. Phys. JETP* **46** (1977) 641;
G. Altarelli, G. Parisi, *Nucl. Phys.* **B126** (1977) 298.

[27] W. Furmanski, R. Petronzio, *Z. Phys.* **C11** (1982) 293.

[28] S. Catani, M. H. Seymour, *Nucl. Phys.* **B485** (1997) 291 and erratum ibid. **B510** (1997) 503 [hep-ph/9605323].

[29] F. Hautmann, *J. High Energy Phys.* **JHEP 10** (2002) 025 [hep-ph/0209320].

[30] C. Duprel *et al.*, *"Comparison of next-to-leading order calculations for jet cross-sections in deep inelastic scattering"* in A. Doyle *et al.* (eds.), Proc. of the Workshop on Monte Carlo Generators for HERA Physics, DESY-PROC-1999-02 (1999) 142 [hep-ph/9910448].

[31] Z. Nagy, Z. Trocsanyi, *Phys. Rev. Lett.* **87** (2001) 082001 [hep-ph/0104315].

[32] D. Graudenz, hep-ph/9710244.

[33] B. Pötter, *Comp. Phys. Commun.* **119** (1999) 45 [hep-ph/9806437].

[34] E. Mirkes, D. Zeppenfeld, *Phys. Lett.* **B380** (1996) 205 [hep-ph/9511448];
E. Mirkes, TTP-97-39 (1997) [hep-ph/9711224].

[35] S. Frixione, Z. Kunszt and A. Signer, *Nucl. Phys.* **B467** (1996) 399 [hep-ph/9512328];
S. Frixione, *Nucl. Phys.* **B507** (1997) 295 [hep-ph/9706545];
see also http://www.ge.infn.it/∼ridolfi/.

[36] H. Jung, *Comp. Phys. Commun.* **86** (1995) 147; version 2.08 is used;
see also http://www.desy.de/∼jung/rapgap.html.

[37] M. Klasen, G. Kramer, *Phys. Rev. Lett.* **93** (2004) 232002 [hep-ph/0410105].

[38] M. Klasen, G. Kramer, *Eur. Phys. J.* **C38** (2004) 93 [hep-ph/0408203].

[39] M. Glück, E. Reya, A. Vogt, *Phys. Rev.* **D46** (1992) 1973;
M. Glück, E. Reya, A. Vogt, *Phys. Rev.* **D45** (1992) 3986.

[40] G. Marchesini, *et al.*, *Comp. Phys. Commun.* **67** (1992) 465;
G. Corcella, *et al.*, *J. High Energy Phys.* **JHEP 01** (2001) 010; version 6.5 is used.

[41] J. Rathsman, *Phys. Lett.* **B452** (1999) 364 [hep-ph/9812423].

[42] A. Edin, G. Ingelman, J. Rathsman, *Comp. Phys. Commun.* **101** (1997) 108 [hep-ph/9605286]; version 6.5.1 is used.

[43] T. Sjöstrand *et al.*, *Comp. Phys. Commun.* **135** (2001) 238 [hep-ph/0010017]; version 6.1 is used.

[44] H. L. Lai *et al.*, *Eur. Phys. J.* **C12** (2000) 375 [hep-ph/9903282].

[45] H1 Collaboration, I. Abt *et al.*, *Nucl. Instrum. Methods* **A386** (1997) 310 and 348.

[46] H1 SpaCal Group, T. Nicholls *et al.*, *Nucl. Instrum. Methods* **A374** (1996) 149; H1 SpaCal Group, T. Nicholls *et al.*, *Nucl. Instrum. Methods* **A386** (1997) 397.

[47] S. Schätzel, Ph.D. Thesis, Univ. Heidelberg, Germany (2004), available from http://www-h1.desy.de/publications/theses_list.html.

[48] H1 Collaboration, C. Adloff *et al.*, *Z. Phys.* **C74** (1997) 221 [hep-ex/9702003].

[49] R. Brun *et al.*, *GEANT 3 User's Guide*, 1987, CERN-DD/EE/84-1.

[50] H1 Collaboration, C. Adloff *et al.*, *Phys. Lett.* **B483** (2000) 36 [hep-ex/0003011].

[51] G. Schuler, T. Sjöstrand, *Phys. Lett.* **B376** (1996) 193 [hep-ph/9601282].

[52] H1 Collaboration, C. Adloff *et al.*, *Eur. Phys. J.* **C13** (2000) 397 [hep-ex/9812024].

[53] M. Bengtsson, T. Sjöstrand, *Z. Phys.* **C37** (1988) 465.

[54] T. Sjöstrand, *Comp. Phys. Commun.* **39** (1986) 347; T. Sjöstrand, M. Bengtsson, *Comp. Phys. Commun.* **43** (1987) 367.

[55] A. Kwiatkowski, H. Spiesberger, H. Möhring, *Comp. Phys. Commun.* **69** (1992) 155.

[56] B. List, Diploma Thesis, Techn. Univ. Berlin, Germany, (1993), unpublished; B. List, A. Mastroberardino, *"DIFFVM: A Monte Carlo Generator for diffractive processes in ep scattering"* in A. Doyle *et al.* (eds.), Proc. of the Workshop on Monte Carlo Generators for HERA Physics, DESY-PROC-1999-02 (1999) 396.

[57] H1 Collaboration, A. Aktas *et al.*, *Eur. Phys. J.* **C48** (2006) 749 [hep-ex/0606003].

[58] F.-P. Schilling, Ph.D. Thesis, Univ. Heidelberg, Germany (2001), available from http://www-h1.desy.de/publications/theses_list.html.

[59] ZEUS Collaboration, J. Breitweg *et al.*, *Eur. Phys. J.* **C1** (1998) 81 [hep-ex/9709021]; ZEUS Collaboration, J. Breitweg *et al.*, *Eur. Phys. J.* **C2** (1998) 237 [hep-ex/9712019].

[60] S. Schenk, Diploma Thesis, Univ. Heidelberg, Germany (2003), available from http://www.physi.uni-heidelberg.de/physi/h1/publications.php.

[61] M. Glück, E. Reya, A. Vogt, *Z. Phys.* **C67** (1995) 433.

Diffractive DIS Dijet Cross Sections

$z_{I\!P}^{\text{jets}}$	$\mathrm{d}\sigma/\mathrm{d}z_{I\!P}^{\text{jets}}$ (pb)	Δ_{stat} (pb)	Δ_{corr} (pb)	Δ_{tot} (pb)	$1 + \delta_{\text{had}}$
$[0.1, 0.4)$	59	5	5	10	1.00 ± 0.03
$[0.4, 0.6)$	34	4	3	8	0.97 ± 0.02
$[0.6, 0.8)$	16	3	2	4	0.95 ± 0.02
$[0.8, 1)$	5.2	1.2	0.6	2.0	1.0 ± 0.2
$\log_{10}(x_{I\!P})$	$\mathrm{d}\sigma/\mathrm{d}\log_{10}(x_{I\!P})$ (pb)	Δ_{stat} (pb)	Δ_{corr} (pb)	Δ_{tot} (pb)	$1 + \delta_{\text{had}}$
$[-2.3, -1.9)$	20.3	2.6	1.5	4.3	1.01 ± 0.02
$[-1.9, -1.7)$	43	5	3	7	0.99 ± 0.01
$[-1.7, -1.5)$	62	7	8	13	0.98 ± 0.04
W (GeV)	$\mathrm{d}\sigma/\mathrm{d}W$ (pb GeV^{-1})	Δ_{stat} (pb GeV^{-1})	Δ_{corr} (pb GeV^{-1})	Δ_{tot} (pb GeV^{-1})	$1 + \delta_{\text{had}}$
$[165, 185)$	0.45	0.06	0.04	0.10	0.95 ± 0.03
$[185, 205)$	0.40	0.05	0.03	0.08	1.00 ± 0.03
$[205, 225)$	0.37	0.05	0.03	0.07	1.00 ± 0.02
$[225, 242)$	0.33	0.05	0.04	0.07	1.03 ± 0.02
Q^2 (GeV^2)	$\mathrm{d}\sigma/\mathrm{d}Q^2$ (pb GeV^{-2})	Δ_{stat} (pb GeV^{-2})	Δ_{corr} (pb GeV^{-2})	Δ_{tot} (pb GeV^{-2})	$1 + \delta_{\text{had}}$
$[4, 6)$	3.4	0.5	0.2	0.7	0.97 ± 0.02
$[6, 8)$	2.4	0.4	0.2	0.5	0.99 ± 0.02
$[8, 12)$	0.83	0.17	0.08	0.21	0.98 ± 0.02
$[12, 20)$	0.63	0.10	0.06	0.14	1.01 ± 0.06
$[20, 30)$	0.47	0.08	0.06	0.12	0.96 ± 0.03
$[30, 40)$	0.18	0.05	0.02	0.06	1.03 ± 0.05
$[40, 80)$	0.081	0.021	0.009	0.026	1.03 ± 0.02

Table 2: The hadron level differential cross section of diffractive dijet production in ep collisions in the DIS kinematic range specified in Table 1. The quoted cross section is the average value over the bin specified in the first column. The quantity Δ_{stat} is the statistical uncertainty, Δ_{corr} the bin-correlated systematic uncertainty and Δ_{tot} the total quadratic sum of statistical and systematic errors including Δ_{corr}. The quantity $1 + \delta_{\text{had}}$ is the factor by which the parton level NLO calculation is multiplied to correct for hadronisation effects.

Diffractive DIS Dijet Cross Sections

$E_T^{*,\mathrm{jet1}}$ (GeV)	$\mathrm{d}\sigma/\mathrm{d}E_T^{*,\mathrm{jet1}}$ (pb GeV^{-1})	Δ_{stat} (pb GeV^{-1})	Δ_{corr} (pb GeV^{-1})	Δ_{tot} (pb GeV^{-1})	$1 + \delta_{\mathrm{had}}$
$[5, 7)$	9.3	0.8	0.6	1.5	1.03 ± 0.01
$[7, 9)$	4.1	0.5	0.4	0.9	0.96 ± 0.01
$[9, 11)$	1.0	0.2	0.2	0.4	0.91 ± 0.09
$\langle \eta_{\mathrm{jet}}^{\mathrm{lab}} \rangle$	$\mathrm{d}\sigma/\mathrm{d}\langle \eta_{\mathrm{jet}}^{\mathrm{lab}} \rangle$ (pb)	Δ_{stat} (pb)	Δ_{corr} (pb)	Δ_{tot} (pb)	$1 + \delta_{\mathrm{had}}$
$[-0.7, -0.4)$	21	3	2	5	0.97 ± 0.06
$[-0.4, -0.1)$	29	4	3	6	1.06 ± 0.03
$[-0.1, 0.2)$	21	3	2	5	1.03 ± 0.02
$\left| \Delta \eta_{\mathrm{jet}}^{*} \right|$	$\mathrm{d}\sigma/\mathrm{d}\left| \Delta \eta_{\mathrm{jet}}^{*} \right|$ (pb)	Δ_{stat} (pb)	Δ_{corr} (pb)	Δ_{tot} (pb)	$1 + \delta_{\mathrm{had}}$
$[0, 0.5)$	30	3	2	5	0.96 ± 0.04
$[0.5, 1)$	15	2	2	3	1.06 ± 0.05
$[1, 2)$	5.9	0.8	0.5	1.3	1.01 ± 0.06

Table 3: The hadron level differential cross section of diffractive dijet production in ep collisions in the DIS kinematic range specified in Table 1 (continued). For details see the caption of Table 2.

Diffractive Photoproduction Dijet Cross Sections

$z_{I\!\!P}^{\text{jets}}$	$\mathrm{d}\sigma/\mathrm{d}z_{I\!\!P}^{\text{jets}}$ (pb)	Δ_{stat} (pb)	Δ_{corr} (pb)	Δ_{tot} (pb)	$1 + \delta_{\text{had}}$
$[0.1, 0.4)$	290	20	30	50	0.85 ± 0.01
$[0.4, 0.6)$	340	20	40	70	0.86 ± 0.02
$[0.6, 0.8)$	310	20	30	50	0.95 ± 0.06
$[0.8, 1)$	150	10	10	30	1.00 ± 0.04
x_{γ}^{jets}	$\mathrm{d}\sigma/\mathrm{d}x_{\gamma}^{\text{jets}}$ (pb)	Δ_{stat} (pb)	Δ_{corr} (pb)	Δ_{tot} (pb)	$1 + \delta_{\text{had}}$
$[0.1, 0.4)$	150	10	20	30	0.69 ± 0.02
$[0.4, 0.6)$	250	20	20	50	0.80 ± 0.02
$[0.6, 0.8)$	370	20	20	40	1.36 ± 0.05
$[0.8, 1)$	350	20	60	70	0.81 ± 0.02
$\log_{10}(x_{I\!\!P})$	$\mathrm{d}\sigma/\mathrm{d}\log_{10}(x_{I\!\!P})$ (pb)	Δ_{stat} (pb)	Δ_{corr} (pb)	Δ_{tot} (pb)	$1 + \delta_{\text{had}}$
$[-2.3, -2.1)$	110	10	10	30	1.13 ± 0.05
$[-2.1, -1.9)$	200	10	20	30	0.94 ± 0.02
$[-1.9, -1.7)$	350	20	30	50	0.88 ± 0.02
$[-1.7, -1.5)$	550	30	60	100	0.84 ± 0.01
W (GeV)	$\mathrm{d}\sigma/\mathrm{d}W$ (pb GeV^{-1})	Δ_{stat} (pb GeV^{-1})	Δ_{corr} (pb GeV^{-1})	Δ_{tot} (pb GeV^{-1})	$1 + \delta_{\text{had}}$
$[165, 185)$	3.8	0.2	0.4	0.6	0.87 ± 0.02
$[185, 205)$	3.5	0.2	0.3	0.5	0.92 ± 0.02
$[205, 225)$	3.0	0.2	0.3	0.4	0.93 ± 0.02
$[225, 242)$	2.4	0.2	0.2	0.4	0.85 ± 0.02

Table 4: The hadron level differential cross section of diffractive dijet production in ep collisions in the photoproduction kinematic range specified in Table 1. For details see the caption of Table 2.

Diffractive Photoproduction Dijet Cross Sections

E_T^{jet1} (GeV)	$\mathrm{d}\sigma/\mathrm{d}E_T^{\mathrm{jet1}}$ (pb GeV^{-1})	Δ_{stat} (pb GeV^{-1})	Δ_{corr} (pb GeV^{-1})	Δ_{tot} (pb GeV^{-1})	$1 + \delta_{\mathrm{had}}$
$[5, 7)$	85	3	7	12	0.85 ± 0.01
$[7, 9)$	28	2	3	4	0.98 ± 0.03
$[9, 11)$	7.3	0.8	1.0	1.9	1.02 ± 0.05
$\langle \eta_{\mathrm{jet}}^{\mathrm{lab}} \rangle$	$\mathrm{d}\sigma/\mathrm{d}\langle \eta_{\mathrm{jet}}^{\mathrm{lab}} \rangle$ (pb)	Δ_{stat} (pb)	Δ_{corr} (pb)	Δ_{tot} (pb)	$1 + \delta_{\mathrm{had}}$
$[-0.7, -0.4)$	140	10	20	30	0.88 ± 0.02
$[-0.4, -0.1)$	230	10	20	30	1.01 ± 0.02
$[-0.1, 0.2)$	190	10	20	30	0.99 ± 0.02
$[0.2, 0.8)$	89	6	7	13	0.79 ± 0.02
$|\Delta \eta_{\mathrm{jet}}|$	$\mathrm{d}\sigma/\mathrm{d}|\Delta \eta_{\mathrm{jet}}|$ (pb)	Δ_{stat} (pb)	Δ_{corr} (pb)	Δ_{tot} (pb)	$1 + \delta_{\mathrm{had}}$
$[0, 0.5)$	179	9	19	29	0.88 ± 0.01
$[0.5, 1)$	157	9	14	21	0.90 ± 0.02
$[1, 1.5)$	88	6	7	13	0.90 ± 0.02
$[1.5, 2)$	55	5	6	9	0.90 ± 0.03
M_{12} (GeV)	$\mathrm{d}\sigma/\mathrm{d}M_{12}$ (pb GeV^{-1})	Δ_{stat} (pb GeV^{-1})	Δ_{corr} (pb GeV^{-1})	Δ_{tot} (pb GeV^{-1})	$1 + \delta_{\mathrm{had}}$
$[9, 17)$	25.6	0.9	2.3	3.9	0.88 ± 0.01
$[17, 27)$	3.8	0.3	0.4	0.7	0.97 ± 0.03

Table 5: The hadron level differential cross section of diffractive dijet production in ep collisions in the photoproduction kinematic range specified in Table 1 (continued). For details see the caption of Table 2.
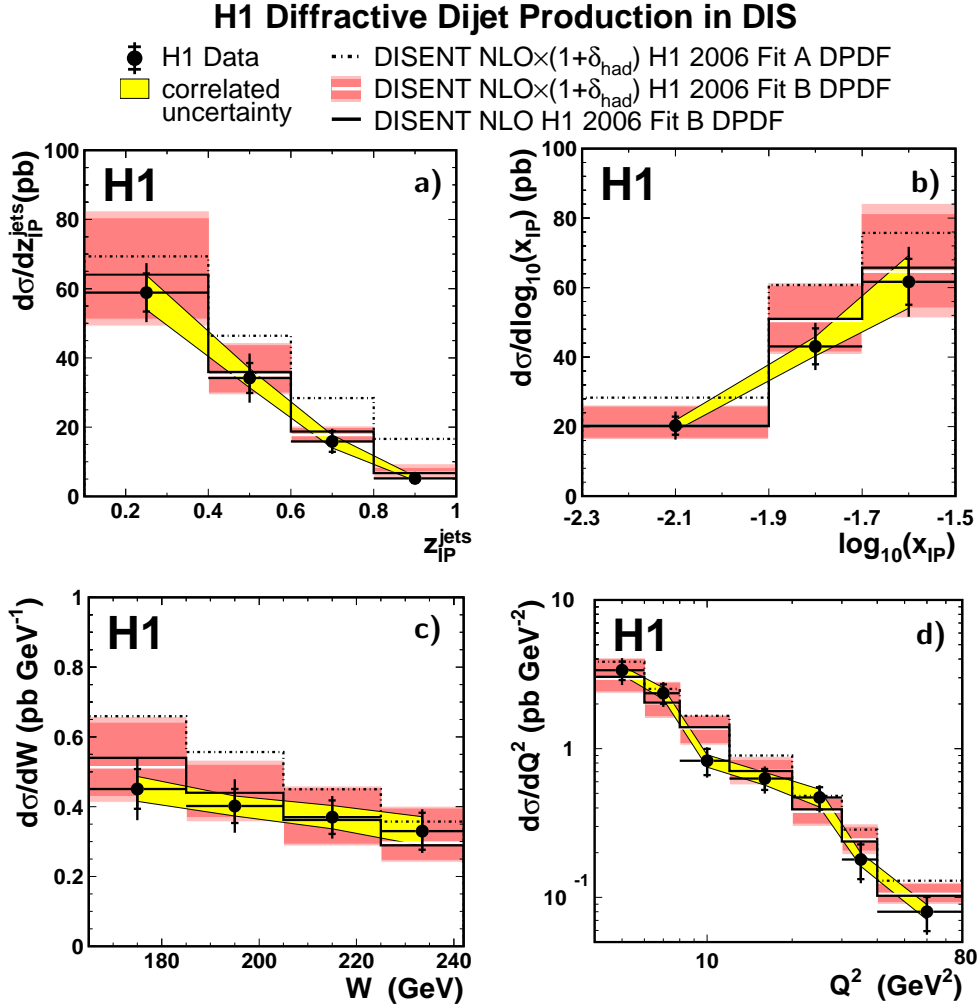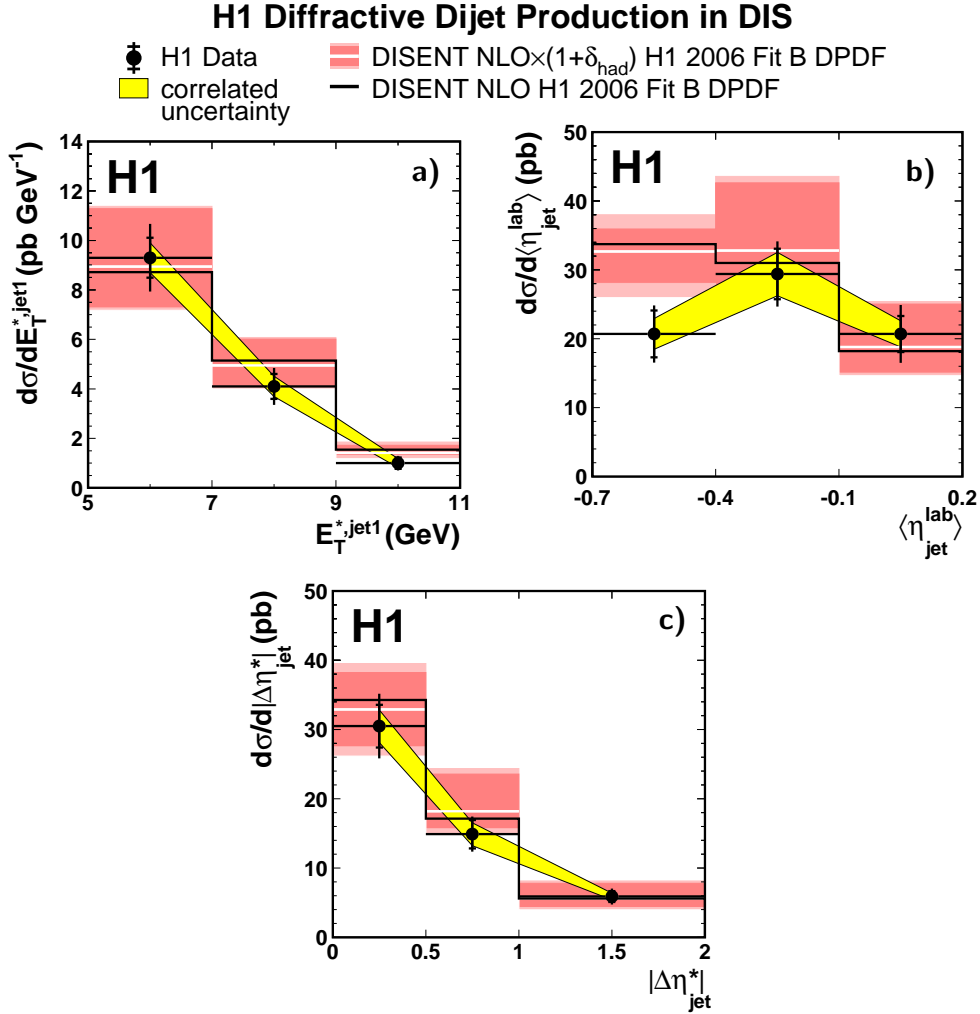
Figure 4: Differential cross sections for the diffractive production of two jets in DIS in the kinematic region specified in Table 1 as a function of a) $z_{I\!P}^{\rm jets}$, b) $\log_{10}(x_{I\!P})$, c) W and d) Q^2. The inner error bars represent the statistical errors. The outer error bars include the uncorrelated systematic errors added in quadrature. The shaded band around the data points indicates an additional systematic uncertainty which is correlated between the data points. The predictions based on the QCD program DISENT, using the 'H1 2006 Fit A' diffractive parton densities and corrected for hadronisation effects are shown as the dash-dotted lines. The predictions based on the 'H1 2006 Fit B' DPDFs are shown both with hadronisation corrections (solid white line) and at the parton level (solid black line). The inner band around the Fit B predictions indicates the uncertainty resulting from the variation of the renormalisation scale by factors 0.5 and 2 and the full band includes the uncertainty due to the hadronisation corrections added linearly.
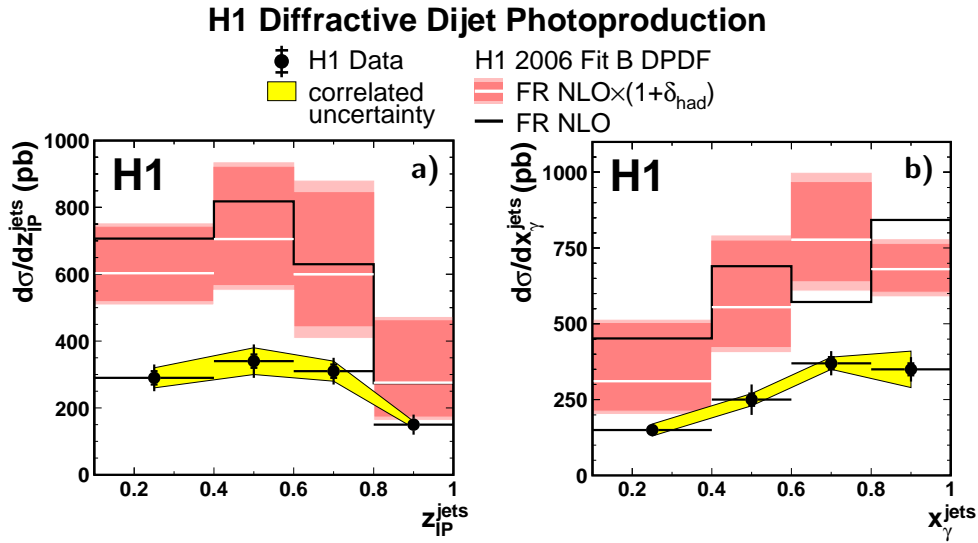
Figure 5: Differential cross sections for the diffractive production of two jets in DIS in the kinematic region specified in Table 1 as a function of the variables a) $E_T^{*,\text{jet}1}$, b) $\langle \eta_{\text{jet}}^{\text{lab}} \rangle$ and c) $\left| \Delta \eta_{\text{jet}}^* \right|$. The DISENT prediction based on the 'H1 2006 Fit B' DPDFs at NLO with (white line) and without (black line) hadronisation corrections is also shown. For details about the errors see the caption of Figure 4.

Figure 6: Differential cross sections for the diffractive production of two jets in photoproduction in the kinematic region specified in Table 1 as a function of a) $z_{I\!P}^{\text{jets}}$ and b) x_{γ}^{jets}. The inner error bars represent the statistical errors, the outer error bars include the uncorrelated systematic errors added in quadrature. The shaded band around the data points indicates an additional systematic uncertainty which is correlated between the data points. The NLO QCD predictions based on the Frixione et al. program (FR) and using the 'H1 2006 Fit B' diffractive parton densities are shown with hadronisation corrections (white line) and at the parton level (black line). The inner band around the NLO prediction indicates the uncertainty resulting from simultaneous variations of the renormalisation and factorisation scales by factors 0.5 and 2 and the full band includes the uncertainty due to the hadronisation corrections added linearly.

H1 Diffractive Dijet Production
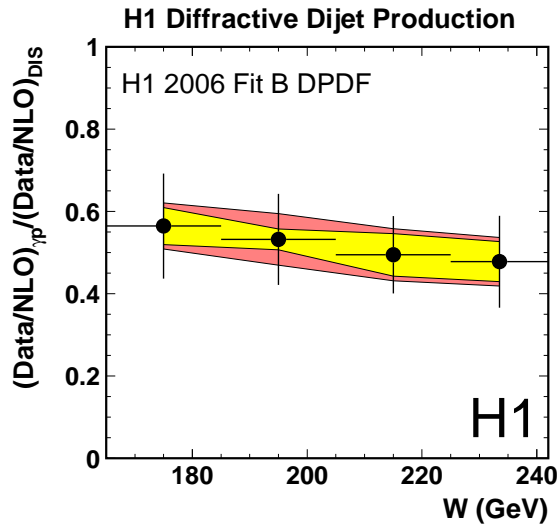
H1 2006 Fit B DPDF

H1

Figure 7: Cross section double ratio of data to NLO prediction for photoproduction and DIS as a function of the photon-proton centre-of-mass energy W. The error bars indicate uncorrelated experimental uncertainties. The error bands around the ratio points show systematic uncertainties which are correlated between the ratio points. The inner band shows experimental uncertainties. The full band shows the quadratic sum of the correlated experimental uncertainties and NLO QCD uncertainties, estimated from variations of the factorisation and renormalisation scales. The nominal QCD scale E_T is varied by the same factors (0.5 and 2) and simultaneously in the same direction for the DIS and photoproduction calculations. The two NLO predictions are based on the same 'H1 2006 Fit B' diffractive parton densities and are corrected for hadronisation effects.
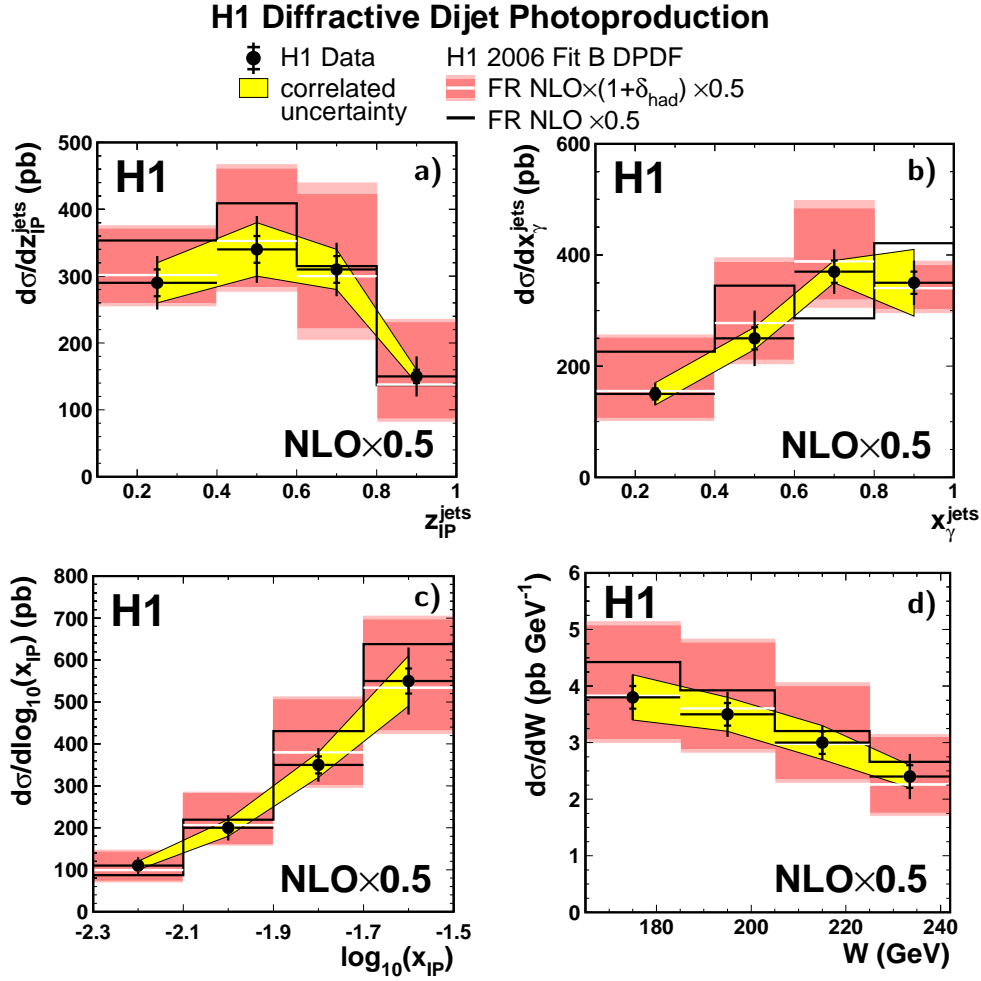
Figure 8: Differential cross sections for the diffractive production of two jets in the photoproduction kinematic region specified in Table 1 as a function of a) $z_{I\!P}^{\mathrm{jets}}$, b) $x_{\gamma}^{\mathrm{jets}}$, c) $\log_{10}(x_{I\!P})$ and d) W. The NLO prediction of the Frixione et al. program interfaced to the 'H1 2006 Fit B' DPDFs with and without hadronisation corrections, scaled by an overall normalisation factor 0.5 is also shown. For details about the errors see the caption of Figure 6.
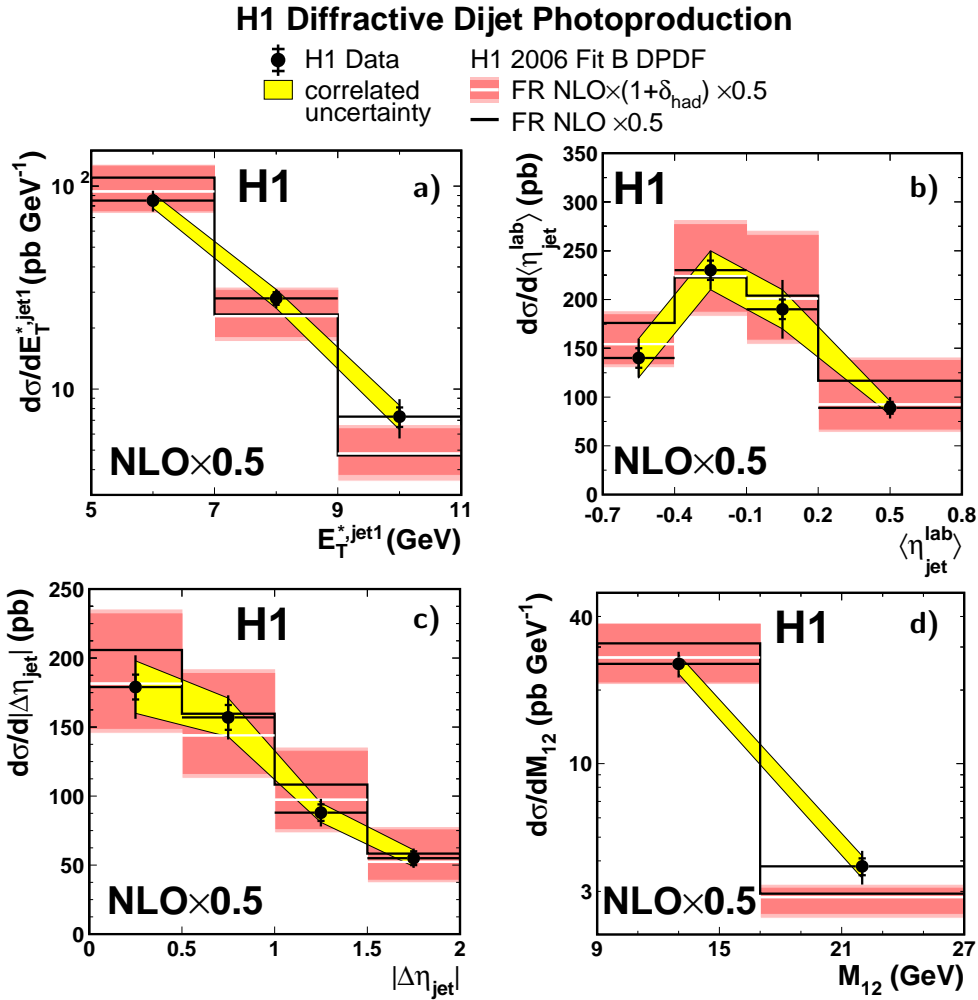
Figure 9: Differential cross sections for the diffractive production of two jets in photoproduction in the kinematic region specified in Table 1 as a function of the jet variables a) E_T^{jet1}, b) $\langle\eta_{\text{jet}}^{\text{lab}}\rangle$, c) $|\Delta\eta_{\text{jet}}|$ and d) M_{12}. The NLO prediction of the Frixione et al. program interfaced to the 'H1 2006 Fit B' DPDFs with and without hadronisation corrections, scaled by an overall normalisation factor 0.5 is also shown. For details about the errors see the caption of Figure 6.
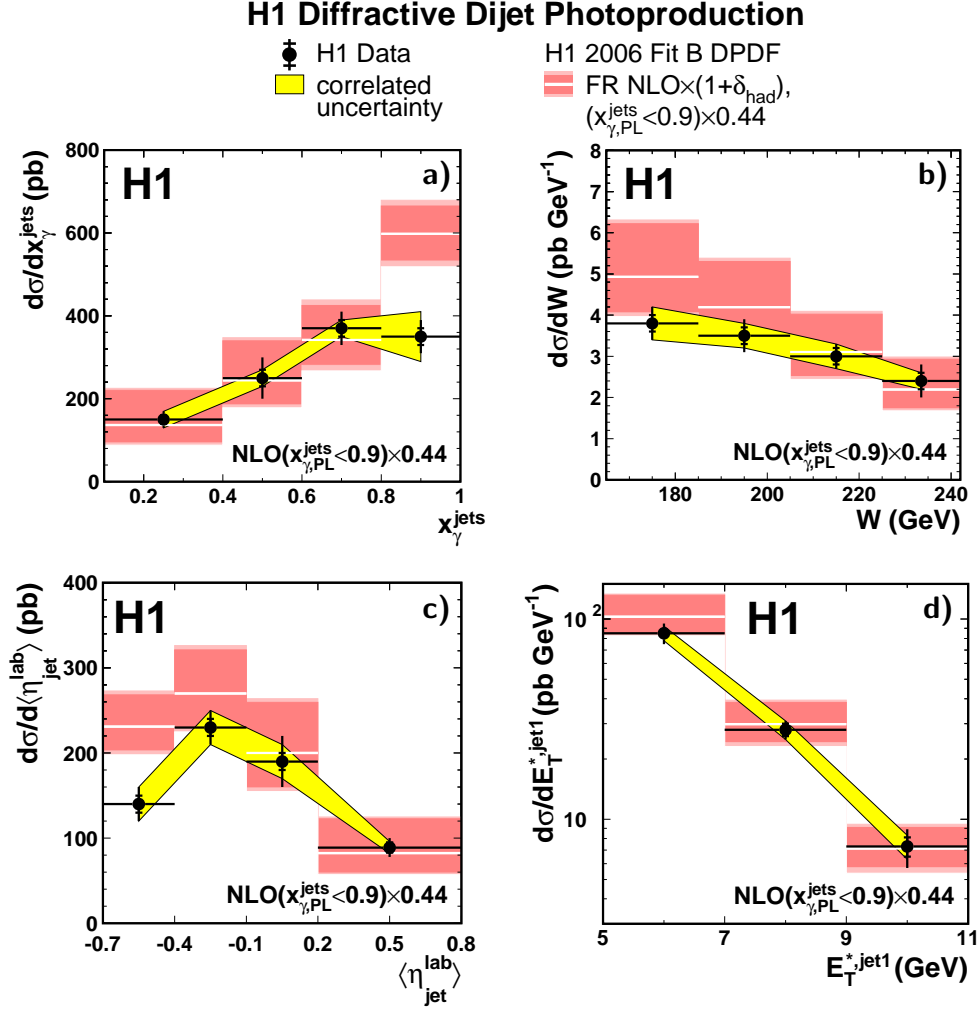
Figure 10: Differential cross sections for the diffractive production of two jets in photoproduction in the kinematic region specified in Table 1 as a function of a) x_γ^{jets}, b) W, c) $\langle \eta_{\text{jet}} \rangle$ and d) E_T^{jet1}. The NLO prediction of the Frixione et al. program interfaced to the 'H1 2006 Fit B' DPDFs with hadronisation corrections is also shown. The part of the NLO calculation for which $x_{\gamma,\text{PL}}^{\text{jets}} < 0.9$ at the parton level is scaled by 0.44. For details about the errors see the caption of Figure 6.
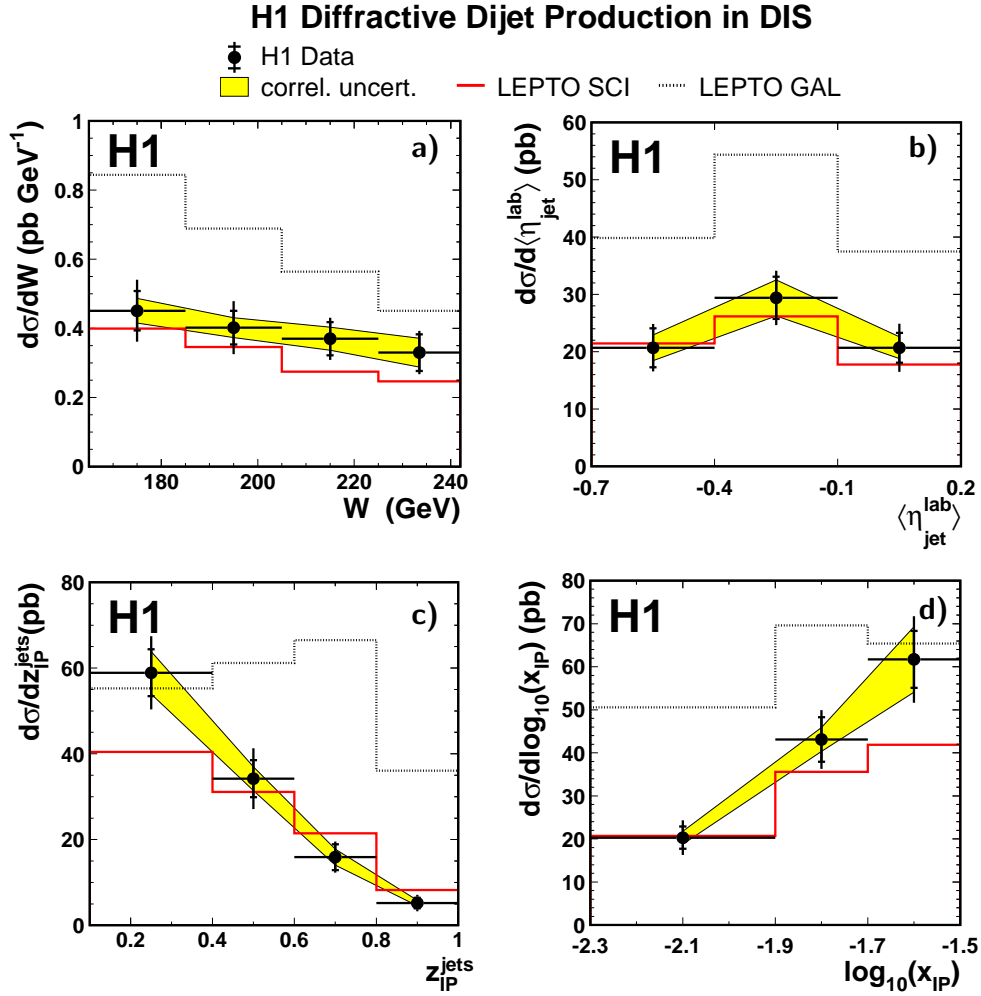
Figure 11: Differential cross sections for the diffractive production of two jets in DIS in the kinematic region specified in Table 1 as a function of the variables a) W, b) $\langle\eta_{\mathrm{jet}}^{\mathrm{lab}}\rangle$, c) $z_{I\!\!P}^{\mathrm{jets}}$ and d) $\log_{10}(x_{I\!\!P})$. Leading order predictions of the soft colour neutralisation models SCI and GAL as implemented in LEPTO are also shown, based on the CTEQ5L leading order proton parton densities. For details about the errors see the caption of Figure 4.
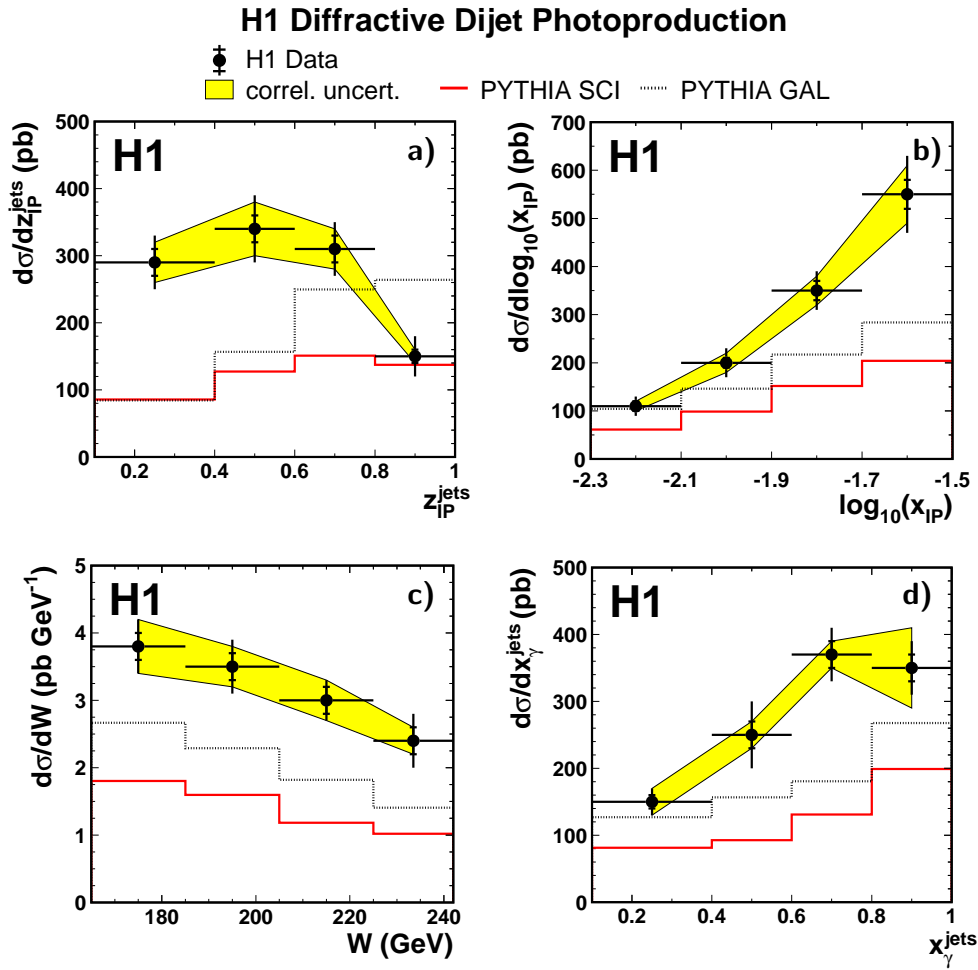
Figure 12: Differential cross sections for the diffractive production of two jets in photoproduction in the kinematic region specified in Table 1 as a function of the variables a) $z_{I\!P}^{\mathrm{jets}}$, b) $\log_{10}(x_{I\!P})$, c) W and d) $x_{\gamma}^{\mathrm{jets}}$. Leading order predictions of the soft colour neutralisation models SCI and GAL as implemented in PYTHIA are also shown, based on the CTEQ5L leading order proton parton densities.